Meteoritics & Planetary Science 33, 1281–1295 (1998)

Asteroid 6 Hebe: The probable parent body of the H-type ordinary chondrites and the IIE iron meteorites

MICHAEL J. GAFFEY[1]* AND SARAH L. GILBERT[2]

[1]Department of Earth and Environmental Science, West Hall, Rensselaer Polytechnic Institute, Troy, New York 12180-3590, USA
[2]National Institute of Standards and Technology, Mail Stop 815.03, 325 Broadway, Boulder, Colorado 80303, USA
*Correspondence author's e-mail address: gaffem@rpi.edu

(Received 1997 March 18; accepted in revised form 1998 August 4)

Abstract–The S(IV)-type asteroid 6 Hebe is identified as the probable parent body of the H-type ordinary chondrites and of the IIE iron meteorites. The ordinary chondrites are the most common type of meteorites falling to Earth; but prior to the present study, no large mainbelt source bodies have been confirmed. Hebe is located adjacent to both the ν_6 and 3:1 resonances and has been previously suggested as a major potential source of the terrestrial meteorite flux. Hebe exhibits subtle rotational spectral variations, indicating the presence of some compositional variations across its surface. The silicate portion of the surface assemblage of Hebe is consistent (both in overall average and in its range of variation) with the silicate components in the suite of H-type chondrites. The high albedo of Hebe rules out a lunar-style space weathering process to produce the weakened absorption features and reddish spectral slope in the S-type spectrum of Hebe. Linear unmixing models show that a typical Ni-Fe metal spectrum is consistent with the component that modifies an H-chondrite spectrum to produce the S-type spectrum of Hebe. On the basis of the association between the H chondrites and the IIE iron meteorites, our model suggests that large impacts onto the relatively metal-rich H-chondrite target produced melt bodies (sheets or pods) that differentiated to form thin, laterally extensive near-surface layers of Ni-Fe metal. Fragments of the upper silicate portions of these melt bodies are apparently represented by some of the igneous inclusions in H-chondrite breccias. Alternately, masses of metal could have been deposited on the surface of Hebe by the impact of a core or core fragment from a differentiated parent body of H-chondrite composition. Subsequent impacts preferentially eroded and depleted the overlying silicate and regolith components, exposing and maintaining large masses of metal at the optical surface of Hebe. In this interpretation, the nonmagmatic IIE iron meteorites are samples of the Ni-Fe metal masses on the surface of Hebe, whereas the H chondrites are samples from between and/or beneath the metal masses.

INTRODUCTION

The ordinary chondrites constitute approximately three-fourths of the modern meteorite falls. The Antarctic meteorite collections indicate that their dominance of the terrestrial meteorite flux has been maintained for at least the past few hundred thousand years. On the basis of analysis of reflectance spectra and other remote sensing data, mineralogically plausible asteroidal parent bodies have been found for most meteorite types (*e.g.*, Gaffey *et al.*, 1993a). On the basis of the additional criterion of an appropriate dynamical delivery process, probable parent bodies have been previously identified for two meteorite classes: asteroid 4 Vesta as the source of the HED (howardites–eucrites–diogenites; basaltic achondrites) suite (Binzel and Xu, 1993) and 3103 Egar (and the Hungaria family) as the source of the aubrites/enstatite achondrites (Gaffey *et al.*, 1992). (In the present paper, we draw attention to the distinction between "plausible parent bodies"—asteroids with the appropriate surface mineralogy for a particular meteorite type—and "probable parent bodies"—asteroids with the appropriate surface mineralogy and whose orbital locations allow delivery of fragments in abundances comparable to the fall frequency of the particular meteorite type.)

However, among nearly 2000 main belt asteroids surveyed, only a single main belt asteroid (3628 Boznemcová; Binzel *et al.*, 1993) is currently recognized as having an ordinary chondrite-like spectrum. (Although several near-Earth asteroids appear to be composed of ordinary chondrite assemblages, their main belt source is not yet identified.) The apparent paradox between the abundance of the ordinary chondrite falls and the rarity of unambiguously similar assemblages among large bodies in the asteroid belt has been a major point of discussion within and between the asteroid and meteorite communities. Various resolutions to this paradox have been proposed, including: (1) that the interpretations of S-type asteroid spectra as mostly differentiated bodies are incorrect due to space weathering effects (*e.g.*, Wetherill and Chapman, 1988; Chapman, 1996); (2) that ordinary chondrites derive from a few rare but favorably situated parent bodies (*e.g.*, Gaffey *et al.*, 1989, 1993b); (3) that ordinary chondrites come from a residual population of small, unheated mainbelt asteroids (Bell *et al.*, 1989); (4) that shock effects darken ordinary chondrite parent body surfaces, disguising them as C-type asteroids (Britt and Pieters 1991, 1994); and (5) that ordinary chondrites come from inner solar system planetesimals ejected to the Oort cloud during planetary accretion and have been recently perturbed into Earth-crossing orbits (Gaffey, 1984).

Although none of these possibilities can yet be rigorously excluded, recent investigations have suggested that the resolution of the apparent paradox lies in some combination of the first three options. Spectral surveys of small mainbelt asteroids (*e.g.*, Xu *et al.*, 1995) are underway that will test the third option. The discovery of an ordinary chondrite-like spectrum for the small (~8 km) mainbelt asteroid 3628 Boznemcová is a result of this survey (Binzel *et al.*, 1993).

The first option has gained support by the observation of spectral and albedo effects attributable to space weathering on the surfaces of the Galileo asteroid flyby targets, Gaspra and Ida-Dactyl. It is observed that the lower albedo regions have a weaker 1 μm absorption

feature and a steeper spectral slope (Chapman *et al.*, 1995). It was concluded that these observations, plus the deep band depth of Dactyl relative to the high albedo regions on Ida, indicate the action of a lunar-style space weathering process (which attains a lesser degree of maturity) on asteroid surfaces. This could help to reconcile the steeper spectral slope and weaker absorption features of undifferentiated S(IV)-type asteroids with ordinary chondrite substrates.

The present paper explores the second option. Based upon mineral compositions derived from the analysis of survey spectra, Gaffey *et al.* (1993b) subdivided the S-asteroid class into seven subtypes based on silicate mineralogy. The survey of the S-type asteroids indicated that the S(IV) subtype of this class has silicate compositions within the ordinary chondrite range (Gaffey *et al.*, 1993b), although most S-asteroids could be rigorously excluded as ordinary chondrite parent bodies on mineralogical criteria. Hebe was classified as a member of subtype S(IV). This subtype exhibits surface silicate assemblages that are either undifferentiated (*i.e.*, chondritic) or only slightly differentiated (*i.e.*, partially differentiated, primitive achondrites such as acapulcoites and lodranites; Takeda *et al.*, 1994; Mittlefehldt *et al.*, 1996; McCoy *et al.*, 1997a,b). The S(IV) subtype was identified as the only subgroup among the S-asteroids that might include ordinary chondrite parent bodies. However, it was noted that such a conclusion did not constitute an identification of S(IV) objects as ordinary chondrite assemblages but only allowed for that possibility. The S(IV)-objects are concentrated near the 3:1 proper motion resonance at 2.5 AU, which provides an efficient escape into Earth-crossing orbits for fragments ejected from objects adjacent to the resonance (*e.g.*, Wisdom, 1985).

Unfortunately, for a simple resolution of the ordinary chondrite parent body question, S(IV) spectra exhibit weaker silicate features and redder spectral slopes than ordinary chondrite assemblages. Although significant uncertainties remain, optical alteration of asteroid surfaces (interpreted from the Galileo images of Ida and Gaspra) has been suggested as a means of reconciling some (or all) of the spectral mismatch between ordinary chondrite and S(IV)-asteroids (option 1). Among the S(IV)-asteroids, and based upon spectral slope, the best candidates for ordinary chondrite parent bodies are asteroids 3 Juno, 6 Hebe, and 7 Iris (Gaffey *et al.*, 1993b). The present paper discusses the results of the spectral evaluation of the leading candidate, 6 Hebe.

ASTEROID 6 HEBE

Hebe is the sixth largest of the 93 member S-asteroid class (Tedesco *et al.*, 1989) with an IRAS diameter of 185 ± 3 km (Tedesco *et al.*, 1992). It has a rotation period of 7.274 h and a complex low amplitude lightcurve (Lagerkvist *et al.*, 1987, 1989). Hebe has an IRAS albedo (0.268 ± 0.008; Tedesco *et al.*, 1992) that is the fourteenth highest of the 93 objects included in Tedesco's S-type class (mean = 0.214, range = 0.127–0.305). Hebe has the fourth lowest UV color and the third lowest v-x color among the 93 S-asteroids. Therefore Hebe is near the limits of the S-asteroid field in these parameters and is a relatively atypical member of the S-type.

Hebe is not a typical S(IV) object. Among the eleven S(IV)-asteroids, Hebe has the second highest albedo (S(IV) range = 0.180–0.277), the lowest UV color, the second lowest v-x color, and the second lowest 0.7–1.5 μm spectral slope (Gaffey *et al.*, 1993b). Hebe is nearly an end member of the S(IV) subtype.

Hebe is located in the inner asteroid belt (orbital elements: a = 2.426 AU, i = 14.8°, e = 0.203) near the 3:1 proper motion resonance with Jupiter at 2.50 AU (Wisdom, 1985) and the ν_6 (or $g = g_6$) secular resonance (located near i = 15–16° at a = 2.426 AU; Williams and Faulkner, 1981). Williams (1973) pointed out that a relatively low ejection velocity (280 m s^{-1}) can place Hebe ejecta into the secular resonance and, thence, into Earth-crossing orbits in $<10^6$ years. Moderate ejection velocities of a few hundred meters per second can deliver relatively large amounts of Hebe fragments into the chaotic zones associated with either of these resonances from whence they can rapidly be transferred into Earth-crossing orbits, which suggests that Hebe is a significant source of meteorites (Farinella *et al.*, 1993a). Based upon the relative efficiency of delivery of impact ejecta to these "escape hatches," Farinella *et al.* (1993b) estimated that Hebe could contribute ~10% (with an uncertainty factor of ~10) of the meteorite flux to the Earth and suggested that this asteroid may be the source of one of the major ordinary chondrite groups. Morbidelli *et al.* (1994) calculated the subsequent orbital evolution of fragments ejected by asteroids located near the ν_6 resonance and confirmed that Hebe should be the most (or one of the most) important contributors to the terrestrial meteorite flux. Migliorini *et al.* (1997) argued from spectral and dynamical considerations that Hebe may be the source of a significant fraction of the ordinary chondrites.

Thus, asteroid 6 Hebe appears to be the best of several potential candidates as one of the long-sought, large, mainbelt ordinary chondrite parent bodies. Dynamical models suggest that Hebe should be a major mainbelt contributor to the terrestrial meteorite flux. Spectral studies indicate that Hebe also has a surface assemblage that allows (or more precisely, does not exclude) an ordinary chondrite affinity.

Observations and Data Reduction

Hebe was observed in 1979 June with the University of Hawaii 2.24 meter telescope atop Mauna Kea using a 2-beam photometer system, a GaAs-C photomultiplier tube, and 25 filters covering the spectral interval 0.33–1.00 μm. The 0.90, 0.93, and 0.96 μm filters were duplicated at the beginning and end of the filter sequence. This photometer is described by McCord (1968). The procedures for reducing the observational data to reflectance spectra and for calibrating and verifying these spectra are discussed in Gaffey (1997). The 1979 observations produced 131 spectra spread throughout the rotational period of Hebe. The average normalized reflectance spectrum of 6 Hebe from these observations is shown on Fig. 1. Figure 2 shows the lightcurve obtained from those data.

The 1979 data showed the presence of rotational spectral variations. Figure 3 shows the relative spectral variations of Hebe for a series of lightcurve segments. The relative spectrum for a nonvarying object would lie along the horizontal line at 1.0 in each case. It is evident that the intensity of the 1 μm absorption feature varies by ~4%—being weakest (above the line) at rotational aspect 0.044–0.165 and strongest (below the line) at rotational aspect 0.379–0.517. The profile of the absorption feature is also changing, because the observed variation is not a simple copy or mirror image of the 1 μm feature shown in the spectrum (Fig. 1).

Chapman *et al.* (1973) observed an equivalent B-V color change of at least 0.05 magnitude and slope changes across the 0.3 to 0.9 μm interval. However, they were not able to determine the lightcurve phasing of these variations. Gehrels and Taylor (1977) showed a 0.02 magnitude (2%) variation in the UV color (~0.43/0.53 μm) in which Hebe was most blue (lowest numerical value of UV color)

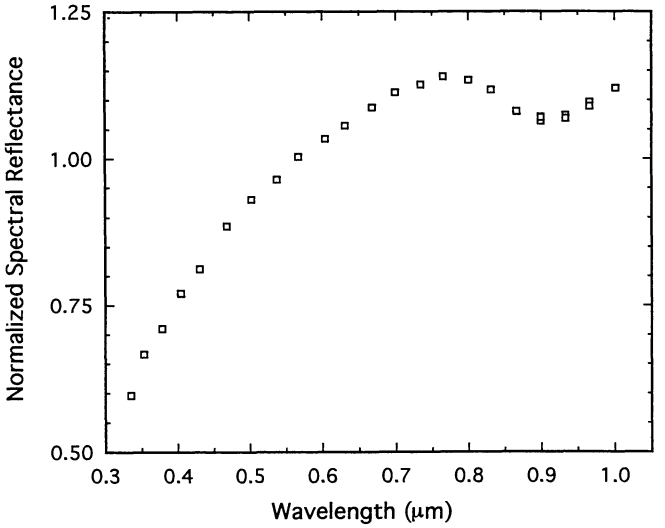

FIG. 1. Average 0.33–1.0 μm reflectance spectrum of 6 Hebe from 131 observations obtained on 1979 June 1–3. The spectrum has been normalized at 0.56 μm. Individual spectra were corrected for lightcurve flux variations prior to averaging. Error bars (standard error of mean) are plotted for all points but are smaller than the plotting symbol. Duplicate measurements of the 0.90, 0.93, and 0.96 μm filters are plotted separately. The primary feature of interest is the mafic silicate absorption feature longwards of 0.76 μm and centered near 0.90–0.93 μm.

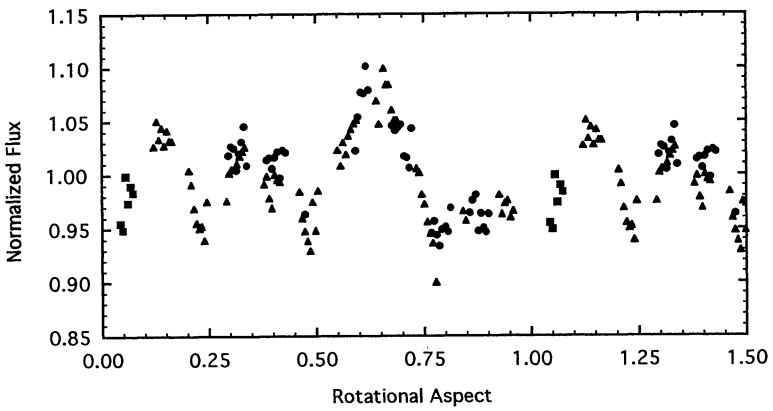

FIG. 2. The lightcurve of 6 Hebe obtained from the 1979 June 1–3 observations. Individual lightcurve points are the average of 17 filters across the 0.40–0.93 μm spectral interval. The lightcurve has been normalized to unity at the overall average. The rotational aspect has been calculated based on the rotational period of 7.274 h with the aspect set to 0.0 at 0 hours UT on 1979 June 1. The observations from 6/1, 6/2, and 6/3 are shown as solid squares, triangles, and circles, respectively. Points for rotational aspect 0.0 to 0.5 are repeated at rotational aspects 1.0 to 1.5.

just past the primary lightcurve maximum (rotational aspect ~ 0.70–0.85), somewhat less blue near the secondary maximum (r.a. ~0.20–0.30) and reddest prior to the primary lightcurve maximum (r.a. ~0.35–0.50). Their observed color variation is approximately equal to that seen between the equivalent wavelengths in Fig. 3. The spectra of Migliorini *et al.* (1997) show similar variations in band intensity and spectral slope at equivalent rotational aspects in their 0.48–0.96 μm CCD spectra. Broglia *et al.* (1994) reported a variation in the optical polarization of Hebe with rotation but concluded that, although their data indicated optical variegation across the surface, it did not require compositional variations. Migliorini *et al.* (1997) also reported rotational variations in the optical polarization of Hebe and reached a similar conclusion. All of the available data sets indicate the presence of reproducible color and spectral variations across the surface of Hebe. Assessment of the compositional significance of these variations requires extended spectral coverage.

Following successful acquisition of 0.33–1.0 μm data, attempts to extend the rotational spectral coverage of Hebe to include the critical 2 μm mafic silicate feature were thwarted by weather and instrument problems during four subsequent oppositions. In 1989 February, rotational coverage of Hebe across the 0.8–2.55 μm spectral interval was finally obtained with the PRIMO double CVF spectrometer on the NASA Infrared Telescope Facility (IRTF) atop Mauna Kea. The instrument and the data reduction procedure have been described in Gaffey *et al.* (1992) and Gaffey (1997), respectively. The observational parameters for both observing runs are listed in Table 1.

The combined average normalized 0.33–2.55 μm reflectance spectrum of Hebe is shown on Fig. 4. In its general properties, this is a typical S-type spectrum with broad weak absorption features centered near 0.9 and 2 μm, a steeply reddish (reflectance increasing with wavelength) spectral curve between 0.33 and 0.75 μm, a shallower rise across the 1 μm feature (between ~0.7 and ~1.4 μm), and a flattening or very shallow rise across the 2 μm feature (between ~1.4 and ~2.5 μm). The absorption features near 1 and 2 μm are due to the mafic silicate minerals, olivine and pyroxene, whereas the reddish spectral curve and the weakness of the absorption features has usually been attributed to spectrally abundant (either physically abundant or finely divided to provide a large surface area) Ni-Fe metal. Some recent workers (*e.g.*, Hiroi *et al.*, 1993; Clark and Hiroi, 1994; Clark, 1995; Clark unpubl. data, 1996) have challenged the Ni-Fe metal interpretation, but the issue remains unresolved. We will return to this question for Hebe.

A primary test of whether Hebe is a differentiated or undifferentiated assemblage utilizes the relative variations in the abundances and compositions of mineral species of the different portions of the asteroid revealed by its rotation (*e.g.*, Gaffey, 1984). For present purposes, undifferentiated (chondritic) assemblages can be considered to have one free variable, oxidation state, such that the compositions and abundances of the major Fe-bearing mineral phases are all correlated (*e.g.*, McSween *et al.*, 1991). Thus, with increasing oxidation across the suite of chondritic meteorites, olivine increases at the expense of Fe metal (Fe^0) and pyroxene, whereas the Fe (Fe^{2+}) content in the mafic silicates increases. The covariance of the mineralogical parameters is expressed as a similar covariance in the spectral parameters.

Lightcurves and Relative Rotational Phase for 1979 and 1989 Observations

Thus, for an asteroid that shows rotational spectral variations (such as those discussed above and shown in Fig. 3), the relative variations in the spectral parameters as a function of rotational aspect provide a means of distinguishing between a differentiated and an undifferentiated assemblage (*e.g.*, Gaffey, 1984). To carry out this test, it is necessary to combine the 1979 and 1989 data by rotational aspect to have a complete 0.33–2.5 μm spectra for different faces of Hebe. This is not as straightforward as might be expected. The relative rotational aspect for observations from the

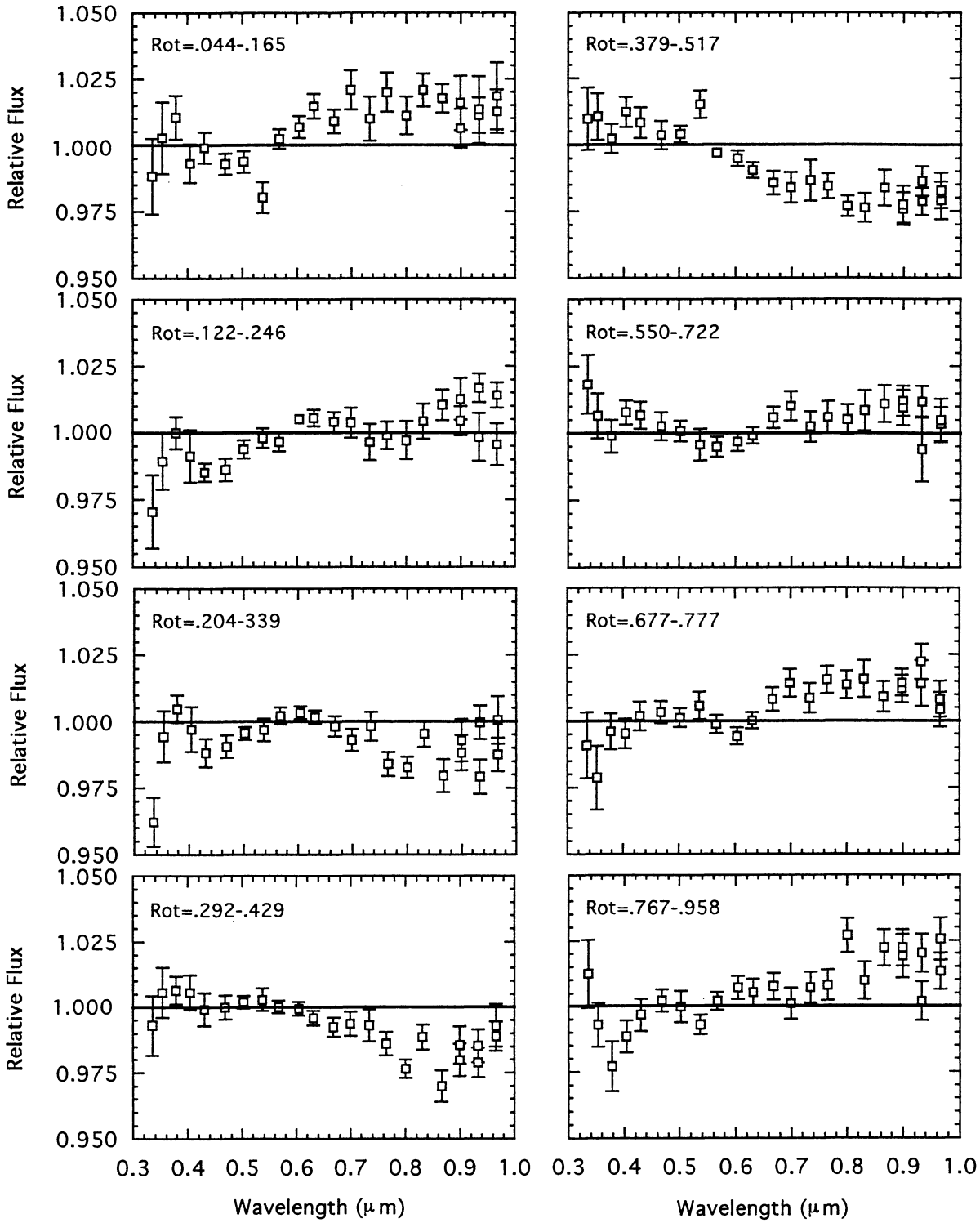

FIG. 3. The relative reflectance spectrum of 6 Hebe for eight lightcurve segments (Fig. 2). In each case, the average reflectance spectrum for the rotational aspect has been divided by the overall average and plotted as the symbols. An object without surface spectral variegation would be unchanging and would plot along the horizontal line at 1.0. The error bars represent the standard error of the mean. Duplicate measurements of the 0.90, 0.93, and 0.96 μm filters have been plotted. The 1 μm point has been omitted because it is considered unreliable due to the rapid falloff in detector sensitivity across the bandwidth of this filter.

earlier and later sets cannot be determined by simply dividing the time interval between observations by the rotation period. The rotation period of Hebe (and most asteroids) is known only to three decimal places. Over a period of several months, this translates to an uncertainty of a significant fraction of a rotation. Over a period of ten years, the uncertainty would be several rotations.

Instead, we were forced to rely on matching features in the lightcurve of Hebe to establish the rotational phase of individual

TABLE 1. Circumstances of Hebe observations.

Date	R.A.	Dec.	V Mag.	Phase Angle	r(AU)	Δ(AU)	Ecliptic Long.	Ecliptic Lat.
6/1/79	16^h 09^m	+01° 49'	9.63	9.01	2.709	1.754	239.7	+22.3
6/2/79	16^h 08^m	+01° 49'	9.64	9.19	2.707	1.755	239.5	+22.3
6/3/79	16^h 07^m	+01° 49'	9.64	9.37	2.705	1.756	239.2	+22.2
2/19/89	08^h 03^m	+17° 12'	9.42	11.91	2.524	1.629	119.2	−3.1
2/20/89	08^h 02^m	+17° 21'	9.44	12.29	2.526	1.638	119.0	−3.0

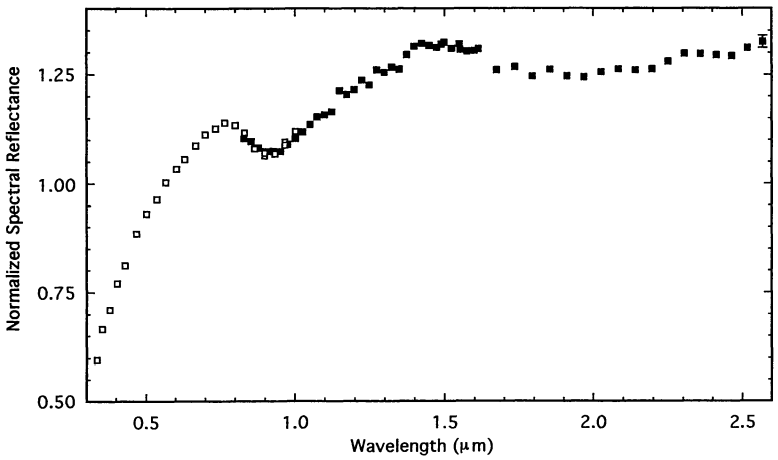

FIG. 4. The average normalized reflectance spectrum of 6 Hebe from the 1979 and 1989 observations. The 1989 data has been normalized to the 1979 data in the overlap region between 0.82 and 0.96 μm. Open squares = 1979; filled squares = 1989.

observations from the two data sets. This is complicated by the fact that the lightcurves from the 1979 and 1989 observation have substantially different amplitudes, ~14% and ~5%, respectively. This is not surprising because the lightcurve amplitude and form is known from previous work to vary substantially for Hebe. Lightcurve shape and amplitude can vary with subearth latitude (*e.g.*, a feature located near the north rotation pole will not contribute to lightcurves obtained at southerly subearth latitudes) and phase angle (amplitudes increase with phase angle).

The lightcurves obtained in the present study are compared with those from four previous studies on Fig. 5a. The subearth latitudes (for four pole determinations, see figure caption) and phase angle of each lightcurve set is indicated. These curves have been stacked in order of subearth latitude from most northerly (top) to most southerly (bottom). The relative changes between lightcurves appear to be primarily a function of the subearth latitude rather than of the phase angle. In general, the amplitude decreases from top to bottom, but the overall features can be recognized between adjacent curves. All curves have been shifted to place the primary lightcurve maximum at rotation ~0.65.

Figure 5b directly compares the lightcurve from 1979 June to that from 1989 February. The amplitude of the 1989 lightcurve has been multiplied by a factor of 3 to make direct comparison easier. The major features are repeated in both lightcurves. The above procedure was used to establish the relative rotational phasing between the individual observations in the 1979 and 1989 data sets that were used in the subsequent analysis. Although this is the most likely rotational phasing, there is the possibility that the actual rotational phase of the 1989 data should be shifted to match one of the other peaks in the 1979 data. The possible effects of this ambiguity on our conclusions are discussed below.

Rotational Spectral Variations

For each of the rotational groups from the 1989 data, the individual observations with corresponding rotational aspects from the 1979 data were averaged together. In several cases, duplicate rotational coverage from the nights of 6/2/79 and 6/3/79 were separately combined with the appropriate 1989 data. The combined 0.335–2.55 μm spectra for each rotational group was then analyzed using the procedures outlined in Gaffey *et al.* (1993b) and Gaffey (1997). Band areas were determined, and the relative areas of the 1 and 2 μm absorption features were calculated, using linear continuum segments tangential to the spectral curve outside the absorption features. The minimum region in each continuum-removed absorption feature was fitted with an N-th order polynomial to determine the wavelength of the band center. The order of the fitting polynomial was the value between 3 and 8 that produced the smallest root mean square residuals. Uncertainties in the band positions were estimated from repeated polynomial fitting of the feature with alternate selections of points and with polynomials of orders other than that which produced the minimum residuals. Due to the weakness of the 2 μm feature (Band II), the determination of its central position is more uncertain than the determination of the position of the 1 μm feature (Band I).

Figure 6 shows the distribution of values of the Band I and Band II centers *vs.* the Band II / Band I area ratio (BAR). The solid line polygons enclose the regions occupied by the ordinary chondrites (OC) and the S(IV)-asteroids. For the Band I position *vs.* BAR plot (Fig. 6a), the overall average (plotted as the large open square) falls in the H-chondrite region of the OC/S(IV) field (see Fig. 7b). The Band I positions *vs.* the BAR for the individual faces and the individual faces from different days are plotted as filled squares and open circles, respectively. The points for these individual faces fall within (or on) the boundary of the lower portion of the OC/S(IV) field, although the uncertainties (especially in the BAR) extend beyond the boundary of the field in some cases. For Band II (Fig. 6b), the mean (large open square) falls in the lower right portion of the OC/S(IV) field but within the H-chondrite region of the field (small symbols). The individual rotation phases scatter above, within, and below the field due to the relatively large uncertainties in the parameter determinations for the weak 2 μm feature.

As noted above, there is potential ambiguity in the relative rotational phase of the 1979 and 1989 data. To check the effects of this ambiguity, the 1989 data was shifted to match its lightcurve maximum (at rotational aspect ~0.65) with the maxima in the 1979 lightcurve (at rotational aspects ~0.15 and ~0.30). The 1979 and 1989 spectra were then combined by rotational groups and the band

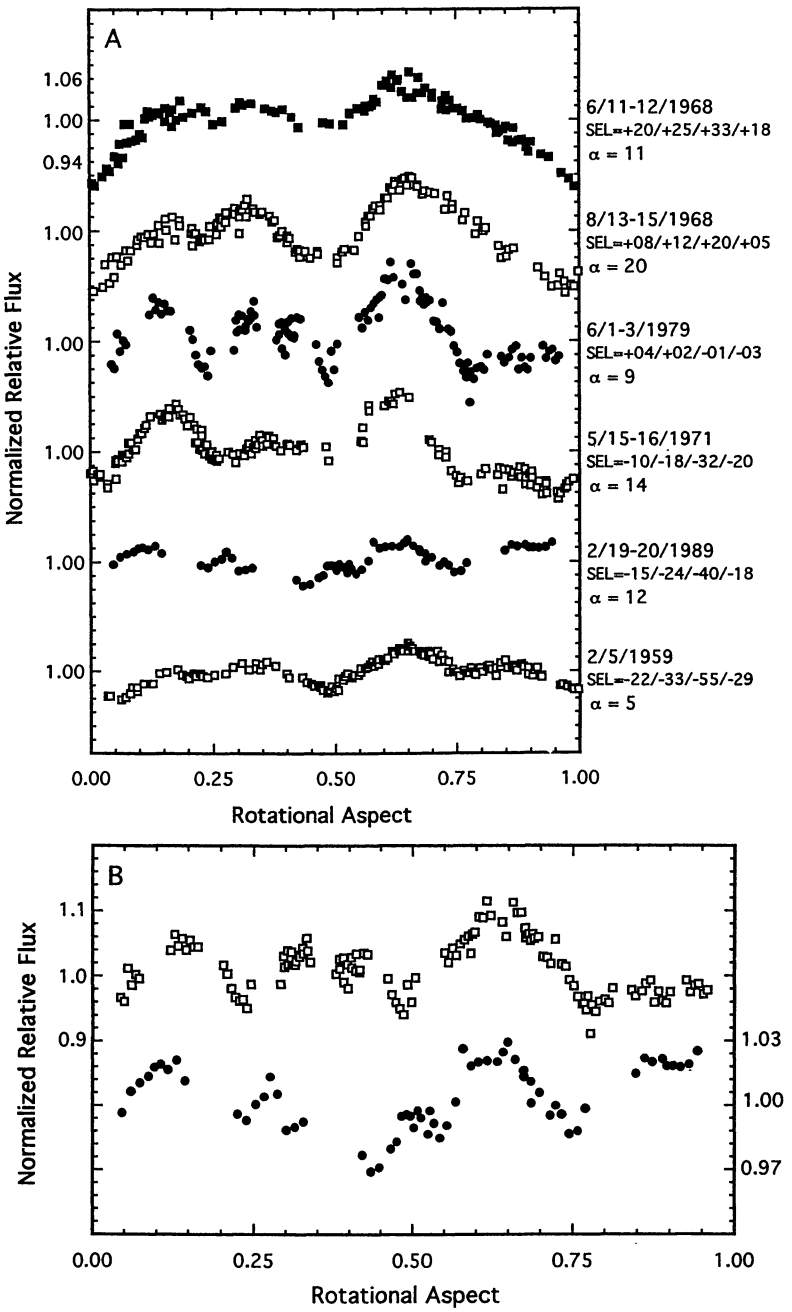

FIG. 5. (a) The lightcurves obtained in the present study (6/1–3/1979 and 2/19–20/1989) compared to previous lightcurves from 6/11–12/1968, 8/13–15/1968, 5/15–16/1971, and 2/5/1959 (Gehrels and Taylor, 1977). The observational subearth latitudes (SEL) for each lightcurve have been calculated for four pole determinations (λ, β) of Hebe (363° and +60°: Michalowski, 1988; 355° and +50°: Magnusson, 1986; 344° and +30°: Zappalà and Knezevic, 1984; 365° and +50°: Gehrels and Taylor, 1977). The phase angle (α) is given for each lightcurve set. (b) Comparison of the lightcurves from 1979 June (open squares) and 1989 February (filled circles) for the rotational phasing used in (a). The amplitude of 1989 lightcurve has been multiplied by a factor of 3 to make direct comparison easier.

centers and areas determined. The derived band position for the 1 μm feature is plotted *vs.* the BAR on Fig. 6c. Although there is a spread to higher BAR values (particularly for the ~0.65 (1989) equals ~0.15 (1979) rotational phasing) and the uncertainties in the band position are often larger, the results are generally consistent with the previous data shown in Fig. 6a. The ~0.65 (1989) equals ~0.15 (1979) rotational phasing appears the least likely, since most (5 of 7) determinations (solid circles on Fig. 6c) have higher band area ratio values than the average spectrum (for which rotational phasing ambiguity is irrelevant).

Figure 7a shows the distribution of parameters for the ordinary chondrite types within the OC/S(IV) field. The H chondrites are toward the "toe" end of this sock-shaped field, L chondrites are concentrated toward the "heel" region, whereas the LL chondrites extend from the "arch" of the foot up to the "ankle." Figure 7b–d shows the distribution of metamorphic subtypes within each chondritic type for parameters from the measured spectra of Gaffey (1976). From H4 to H6, there is a shift from right to left. The L4 to L6 points exhibit a similar behavior displaced to the left of the corresponding H-types. The shift from grade 4 to 6 for the LL meteorites is up and left.

The general region within the S(IV) field occupied by each of the ordinary chondrite types is a manifestation of differences in their mineralogies. In addition, the variation in trends of metamorphic grades for each OC type is a function of systematic variations in mineralogy due to oxidation during metamorphism (McSween and Labotka, 1993). Figure 7e shows the average spectral parameters calculated from the mean mineral abundances and compositions of the metamorphic subtypes of each OC group measured by McSween and Labotka (1993), using the relationships between spectral parameters and mineralogy derived by Cloutis *et al.* (1986). The calculated spectral parameters shown in Fig. 7e exhibit the same spatial relationships and metamorphic trends shown by the measured spectral parameters of the OC groups in Fig. 7b–d. The calculated metamorphic ranges are shorter than the trends in the measured data, because the former is derived from averages, whereas the latter represents individual specimens sampling some portion of the range of variation within each type.

The Band II/Band I area ratios for the average spectrum of Hebe—and for most of the individual faces of Hebe (Fig. 6a)—overlie the H-chondrite region. The spread in the BARs for Hebe spans the range from H4 to H6 and extends somewhat beyond this range. The Band I *vs.* BAR and the BII *vs.* BAR points for the average Hebe spectrum fall in the H5/H6 portion of the H-chondrite region (compare Fig. 6a to Fig. 7b and compare the average Hebe point to the H-chondrite points in Fig. 6b).

Within the uncertainties of the measurements, the silicate mineralogy of asteroid 6 Hebe appears consistent with that present in the H-chondrite suite, in terms of both the average and the variation. The data for Band II (Fig. 6b) are consistent with this interpretation but are too noisy to provide additional constraints. It is also evident that the Hebe silicates are well distinguished from basaltic assemblages (BAR = 1.55 to 2.7; Gaffey *et al.*, 1993b), which would be expected for a previous interpretation of the short wavelength spectrum (0.4–1.1 μm) of Hebe as indicating a mesosiderite assemblage (Gaffey and McCord, 1979). In the Hebe data, there is no persuasive indications of assemblages outside the H-chondrite range, nor is there indication of magmatic differentiation.

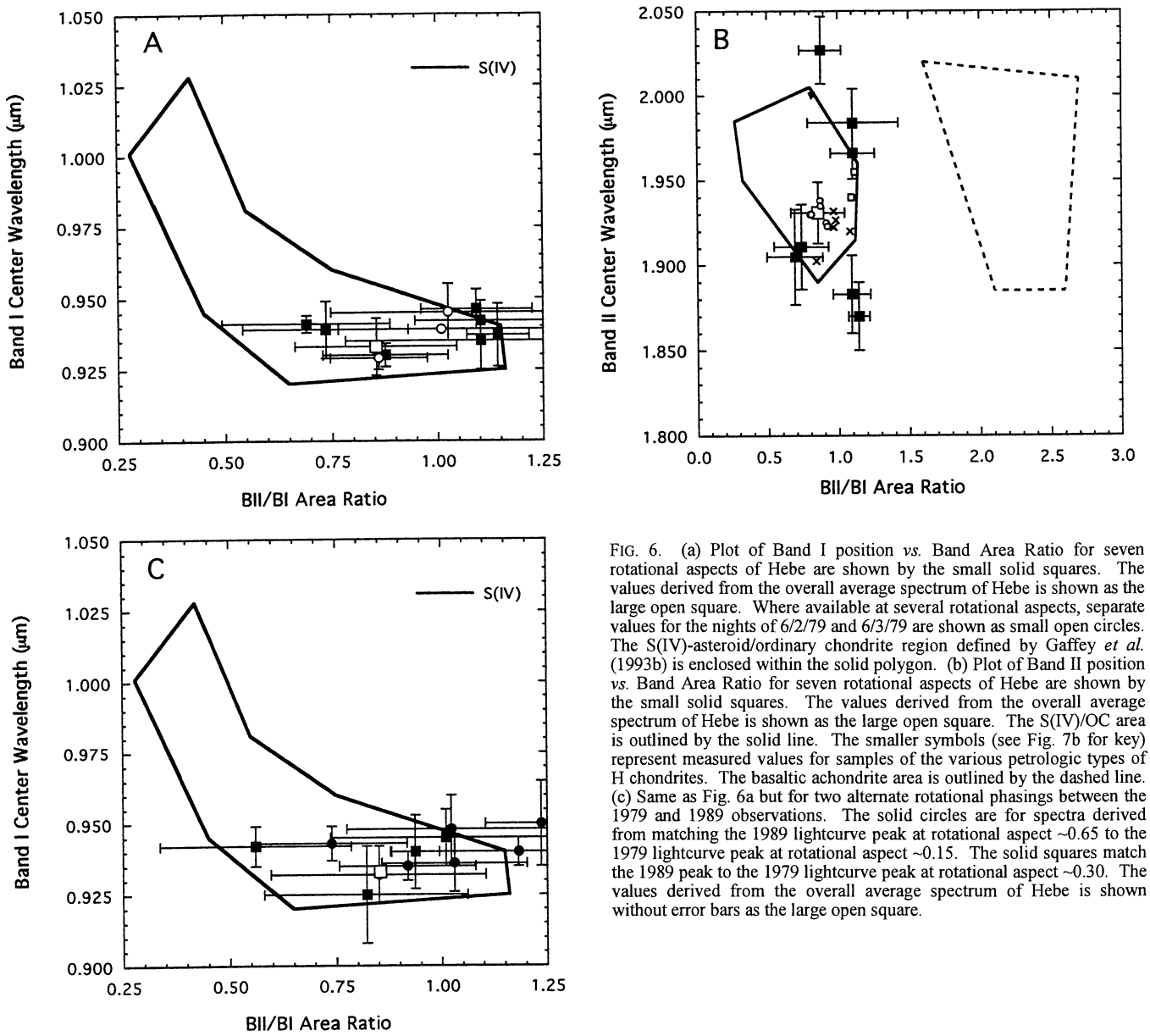

FIG. 6. (a) Plot of Band I position *vs.* Band Area Ratio for seven rotational aspects of Hebe are shown by the small solid squares. The values derived from the overall average spectrum of Hebe is shown as the large open square. Where available at several rotational aspects, separate values for the nights of 6/2/79 and 6/3/79 are shown as small open circles. The S(IV)-asteroid/ordinary chondrite region defined by Gaffey *et al.* (1993b) is enclosed within the solid polygon. (b) Plot of Band II position *vs.* Band Area Ratio for seven rotational aspects of Hebe are shown by the small solid squares. The values derived from the overall average spectrum of Hebe is shown as the large open square. The S(IV)/OC area is outlined by the solid line. The smaller symbols (see Fig. 7b for key) represent measured values for samples of the various petrologic types of H chondrites. The basaltic achondrite area is outlined by the dashed line. (c) Same as Fig. 6a but for two alternate rotational phasings between the 1979 and 1989 observations. The solid circles are for spectra derived from matching the 1989 lightcurve peak at rotational aspect ~0.65 to the 1979 lightcurve peak at rotational aspect ~0.15. The solid squares match the 1989 peak to the 1979 lightcurve peak at rotational aspect ~0.30. The values derived from the overall average spectrum of Hebe is shown without error bars as the large open square.

Reconciling the S-Type Spectrum of Hebe with an H-Chondrite Assemblage

What progress have we made? Although the silicate fractions of Hebe's surface assemblage appear identical to those in H chondrites, how do we account for the weak spectral features and reddened spectral slope of Hebe? These characteristics of S-type spectra have been long recognized as a barrier to identification of S-asteroids as OC parent bodies (*e.g.*, Chapman and Salisbury, 1973; McCord and Gaffey, 1974; Gaffey and McCord, 1979; Feierberg *et al.*, 1982; Gaffey, 1986; Wetherill and Chapman, 1988; Bell *et al.*, 1989; Gaffey *et al.*, 1989, 1993b). A number of models have been proposed to reconcile S-type spectral properties with ordinary chondrite assemblages, including abundant fine-grained metal in the surface regolith produced by impact fracturing of metal grains (*e.g.*, Feierberg *et al.*, 1982) and a lunarlike space weathering process (*e.g.*, Wetherill and Chapman, 1988; Chapman, 1996). Although the first alternative has been eliminated (*e.g.*, Gaffey, 1986), the second alternative has recently gained support from the Galileo images of mainbelt S-asteroids Gaspra and Ida/Dactyl (*e.g.*, Chapman *et al.*, 1995).

The lunar space weathering process weakens the absorption features, reddens the spectrum, and lowers the albedo. The operation of a weaker version of the lunar space weathering process on asteroid surfaces is proposed from the Galileo asteroid images (Chapman *et al.*, 1995; Chapman, 1996). Figure 8 compares the spectral albedo curve of Hebe to that of the average of the H6 chondrites (Gaffey, 1976). The albedo of Hebe is higher at all wavelengths than that of the average of the H6 chondrites that have the highest albedos (and spectral albedos) of the H-chondrite suite. So, although the spectrum of Hebe exhibits the weak absorption features and reddened spectral curve characteristic of S-asteroids, its albedo is equal to or higher than the brightest of the appropriate chondrite analogues.

The 1 μm band depth in the Hebe spectrum is ~6.5% (relative to the reflectance peak near 0.75 μm) or ~9.5% (relative to a linear

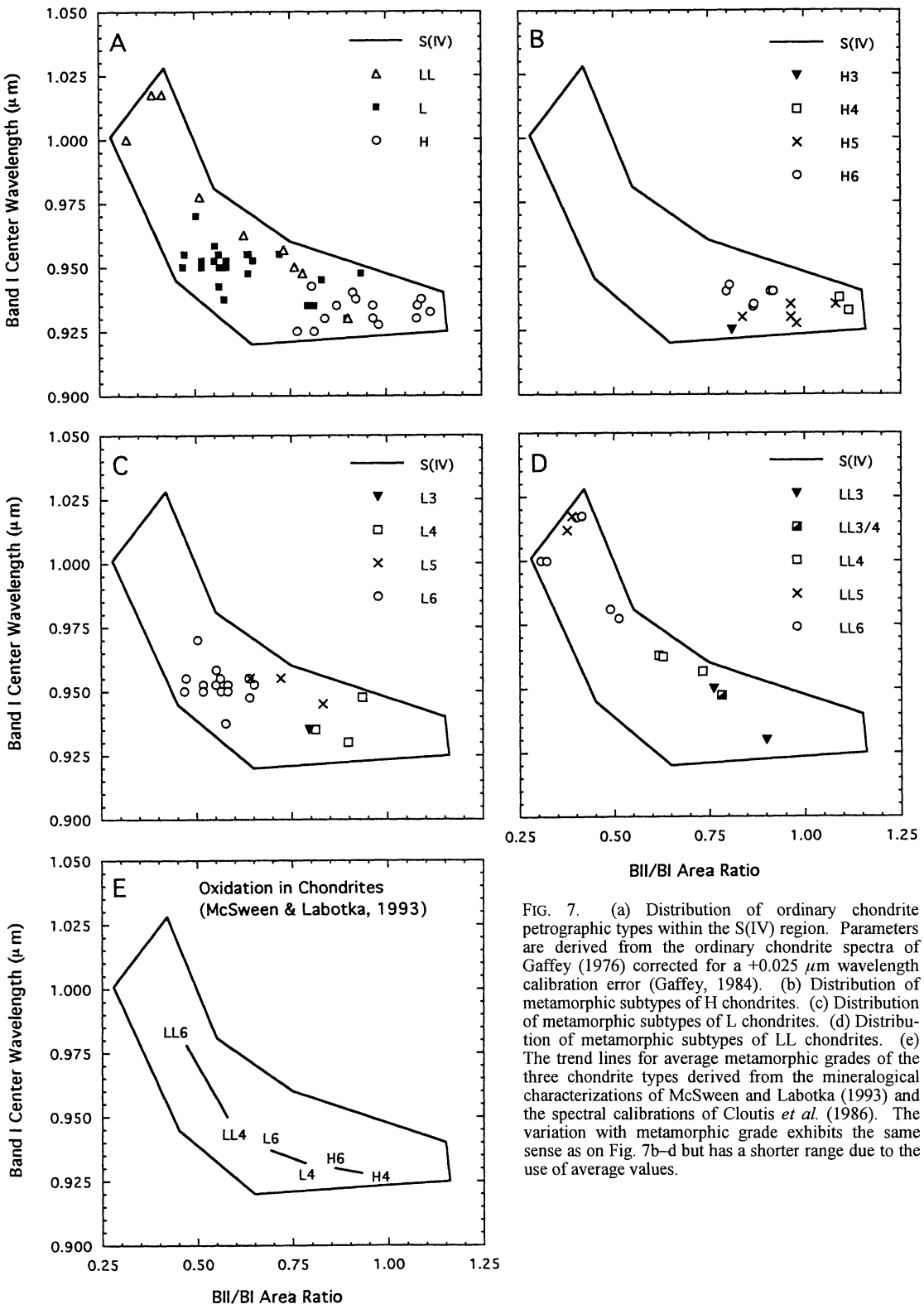

FIG. 7. (a) Distribution of ordinary chondrite petrographic types within the S(IV) region. Parameters are derived from the ordinary chondrite spectra of Gaffey (1976) corrected for a +0.025 μm wavelength calibration error (Gaffey, 1984). (b) Distribution of metamorphic subtypes of H chondrites. (c) Distribution of metamorphic subtypes of L chondrites. (d) Distribution of metamorphic subtypes of LL chondrites. (e) The trend lines for average metamorphic grades of the three chondrite types derived from the mineralogical characterizations of McSween and Labotka (1993) and the spectral calibrations of Cloutis *et al.* (1986). The variation with metamorphic grade exhibits the same sense as on Fig. 7b–d but has a shorter range due to the use of average values.

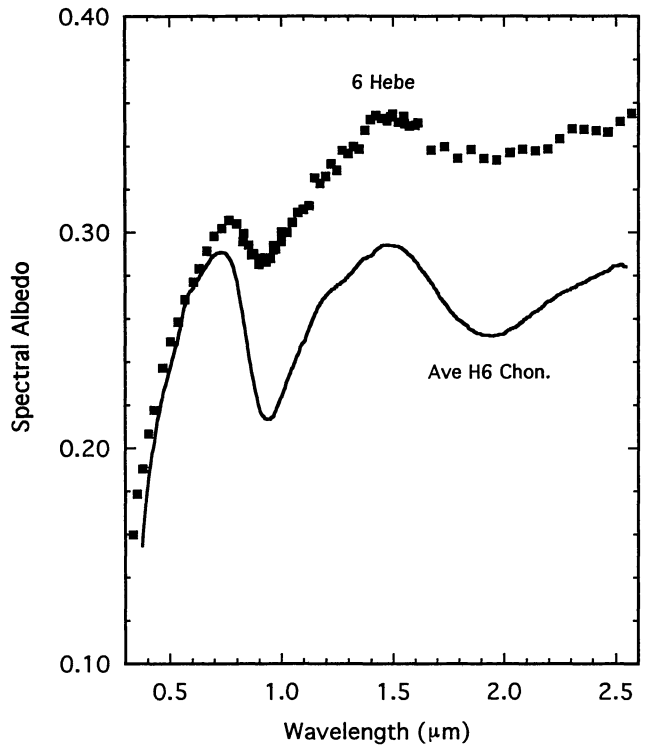

FIG. 8. Spectral albedo curve of 6 Hebe compared to that of an average of the H6 chondrite spectra in Gaffey (1976). The spectral albedo curve of Hebe was produced by multiplying the normalized spectral reflectance curve of Hebe (Fig. 4) by the IRAS albedo of Hebe (0.268; Tedesco *et al.*, 1992).

continuum fitted at ~0.75 and ~1.30 μm) and can be compared to the band depth for the average H6 chondrite of ~27%. The band in the Hebe spectrum is 3–4× weaker than the band in the H6 chondrite spectrum. The correlation between band depth and albedo as a function of the degree of space weathering has been explored for several different proposed space weathering mechanisms. Fischer and Pieters (1994) showed the change in band depth and albedo for various lunar soils as a function of the exposure index I_s/FeO. Depending on the specific landing site sample used (*i.e.*, bulk composition), decreasing the band depth to 25–33% of the original value was coupled with a decrease in the albedo to ~50% of the initial value. Clark *et al.* (1992) measured the spectral effects of melting, comminution, and recrystallization on chondrites. Their values of band depth and albedo would indicate that a three to fourfold decrease in band depth would produce a two to threefold decrease in albedo. Moroz *et al.* (1996) used a laser to produce rapid heating and cooling of an ordinary chondrite and meteorite-type silicates to simulate space weathering on asteroid surfaces. For an L5 chondrite, an olivine and an olivine–clinopyroxene mixture, they showed that the albedo and band depth decreased at approximately the same rate. Keil *et al.* (1992) measured the spectra of dark (shock blackened) clasts to light (unshocked or lightly shocked) clasts in the same chondrite specimens. Although they did not quantify the changes in absorption band depth, it is clear that the albedo and band intensity decrease together. Similarly, Britt and Pieters (1994) show a correlated decrease in band depth and albedo for shocked chondrites relative to unshocked chondrites. Thus the high albedo of Hebe would appear to rule out either a lunar-type space weathering process, silicate melting, or shock as the cause of the weakened features in the Hebe spectrum. (To produce the weakened features in the Hebe spectrum by the weathering mechanisms discussed above, the initial albedo of the albedo of the unweathered material would be 50–60%, which is far above the ordinary chondrite range.) Comparison of the Hebe spectrum to lower metamorphic grade chondrites (*e.g.*, H5, H4, or H3), which have weaker absorption features (*e.g.*, Fig. 16c in Gaffey, 1976), only increases the albedo discrepancy.

If the surface of Hebe includes H-chondrite assemblages, then the mechanism that modifies the OC spectrum to an S-type spectrum must weaken the features, redden the slope, and either not effect or increase the albedo. The traditional candidate to redden the spectrum of Hebe is an abundant, coarse-grained Ni-Fe metal component in the surface material. This is supported by a simple unmixing exercise. If one assumes a coarse metal component, then the surface can be modeled by a linear (or checkerboard) model, in which individual photons interact with silicate or with metal, but seldom with both. (By contrast, intimate mixtures of finer grain sizes, where individual photons commonly interact with both species, require more complex mixing models. As Cloutis *et al.* (1990) showed, increasing metal content in intimate metal–silicate mixtures substantially lowers the albedo of the resulting assemblage. The albedo of Hebe, therefore, argues for the simple linear mixing model.) In this exercise, a spectral contribution from an H6 chondrite, corresponding to a fraction of the surface (*e.g.*, 30%), was subtracted from the Hebe spectral albedo curve. This process was repeated until the residual exhibited no 1 μm silicate absorption feature. This spectral unmixing process was repeated with an average H5 spectrum. The resulting residual spectrum is the spectral albedo curve of an agent whose presence would modify an H-chondrite surface material to produce the S-type spectrum of Hebe.

Figure 9 shows the residual spectra resulting from the spectral unmixing of average H5 and H6 chondrite spectra from the Hebe spectrum. Both of these curves are consistent with the range of slopes, curvatures, and albedos exhibited by the nickel-iron meteorites. (The cause of the flattening of the spectral curve of some (but not all) Fe and Ni-Fe samples and of the Hebe reddening agent is not known but is a topic of considerable interest, for example, Gaffey 1976, 1986; Hiroi *et al.*, 1993; Clark and Hiroi 1994; Clark 1995, unpubl. data, 1996.) The H5 model corresponds to a surface with 60% H5 chondrite and 40% Ni-Fe metal. The H6 model corresponds to a surface with 40% H6 chondrite and 60% Ni-Fe metal. Because the mean for Hebe falls in the H5 area and the variation for Hebe spans the H-chondrite range (Fig. 6a), the H5 model is preferred. Thus, the favored interpretation is that the surface of Hebe consists of a coarse (equal to or greater than centimeter scale) areal mixture of ~60% H-chondrite material with ~40% Ni-Fe metal.

Farinella *et al.* (1993b) provide additional support for the identification of Hebe as the H-chondrite parent body. They noted that among three meteorites for which preterrestrial orbits have been established, one (Příbram) has an orbit that is consistent with derivation from the ν_6 resonance near the location of Hebe. Příbram is an H5 chondrite.

ORIGIN OF THE HEBE SURFACE ASSEMBLAGE

At first glance, it might appear that no progress has been made. It has long been suggested that an abundant Ni-Fe metal component could transform an ordinary chondrite spectrum into an S-type spectrum (*e.g.*, Feierberg *et al.*, 1982). The problem has been how to produce the enhanced metal abundance with an undifferentiated assemblage (*e.g.*, Gaffey, 1986). In the case of 6 Hebe, a solution to

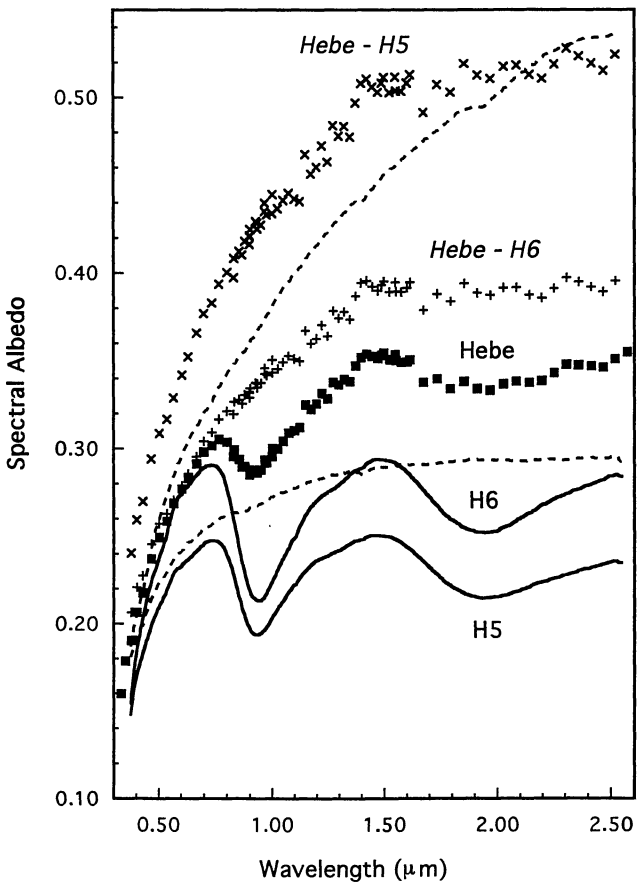

FIG. 9. Residual spectra resulting from the spectral unmixing of average H6 and H5 spectra from the Hebe spectrum. The residual spectra were calculated for the same wavelengths as the Hebe spectrum. The average H5 and H6 spectra are shown as well as the spectra of two iron meteorites (dashed lines) from Gaffey (1976). Although iron-nickel meteorites consistently exhibit reddish (*i.e.*, reflectance increasing with wavelength) spectral curves, there is considerable variation in the albedo and curvature of the spectrum. The iron-nickel meteorite spectra shown here represent the range of variation in Gaffey (1976).

this dilemma lies in the association of the IIE iron meteorites with the H-chondrite parent body (or with that parent body's chemical, isotopic, and mineralogical twin).

The IIE iron meteorites are classed as nonmagmatic irons (Wasson and Wang, 1986). Most iron meteorites were formed by magmatic differentiation during complete melting or extensive partial melting of their parent bodies and appear to be derived from the cores of those bodies (*e.g.*, Taylor, 1992). By contrast, the nonmagmatic IIE iron meteorites were apparently formed near the surfaces of their parent bodies, either by metal–silicate segregation in melt masses produced by large impacts or by impact of metallic material (either initially molten or melted by the impact) onto the surface of a H-type chondritic parent body (*e.g.*, Wasson and Wang, 1986; Olsen *et al.*, 1994; Casanova *et al.*, 1995). The presence of relatively abundant silicate inclusions in nonmagmatic iron meteorites indicates that metal–silicate segregation was incomplete, which is consistent with a relatively rapid cooling, probably as a near-surface melt.

The various IIE iron meteorites were formed in several events during the first seven hundred million years of solar system history (Dodd, 1981; Olsen *et al.*, 1994). This is consistent with their origin in discrete impact events on their parent body, because impact heating is the only available heat source for most asteroids that extends beyond the first few million years of solar system history (*e.g.*, Scott *et al.*, 1989). Impact melting has been an important process on a number of meteorite parent bodies (*e.g.*, Rubin, 1995, and references therein). For example, the L-chondrite Chico is composed of ~60% impact melt produced during a major impact event onto the L-chondrite parent body 500 Ma ago (Bogard *et al.*, 1995). Yolcubal *et al.* (1997) concluded (from the study of igneous inclusions in seven heavily shocked chondrites) that in some cases, the impact melts were sufficiently long-lived to allow partial olivine segregation to occur. Metal would segregate from such melts much faster than olivine, indicating the potential to form sheets or pods of metal.

The silicate inclusions in the IIE iron meteorites have O isotopes that fall in the H-chondrite field and lie on the H-chondrite fractionation line (Clayton *et al.*, 1983, 1991). Most of the silicate inclusions in the IIE iron meteorites are partial melts obscuring their original nature, but several preserve an H-chondrite chemical signature or petrology (Olsen *et al.*, 1994; Casanova *et al.*, 1995). Ebihara *et al.* (1996) describe a IIE iron specimen that was originally classified as an H6 chondrite and that contains a silicate portion compositionally and petrologically similar to either an H5 or H6 chondrite. They proposed formation on the surface of the H-chondrite parent body from intrusion of H-chondrite country rock by a metal–sulfide melt derived from impact melting of H-chondrite material.

The high density of Ni-Fe–FeS melt, relative to chondritic silicates, increases the efficiency of the metallic phase segregation from an impact melt. Higher abundances of metal in a silicate–metal melt increases the growth rate of metal melt globules by mutual collision and merging of smaller droplets. Larger metal globules settle more rapidly, increasing the rate and efficiency of metal–silicate segregation (*e.g.*, Taylor, 1992). Because of the relatively high abundance of Ni-Fe metal in H-chondrite material (average = 18.0 wt%, range = 14.3–21.4%; McSween *et al.*, 1991), the formation of a significant metal layer in impact melts generated on an H-chondrite substrate should be much easier than on L-chondrite (8.4%, 5.4–10.5%) or LL-chondrite (3.6%, 1.4–7.9%) substrates. (Rubin *et al.* (1986) describe an ungrouped iron meteorite, Guin, which resembles the IIE iron meteorites but, based on O isotopes, is not related to the IIE iron meteorites or the H chondrites. Instead, Guin has O isotopes that lie along a fractionation line through the L chondrites and that lies at the edge of the LL-chondrite field. This suggests that the proposed mechanism may also work for L- and LL-chondritic materials.) A schematic model of the impact-melt formation of Ni-Fe metal layers on the H-chondrite and IIE iron parent body is shown at the top of Fig. 10.

Craters up to 8 km in diameter were observed on Ida (Belton *et al.*, 1994), an asteroid approximately one-sixth the diameter of Hebe. Images of asteroid 253 Mathilde (66 × 48 × 46 km) showed five large craters (diameters from 19 to 33 km) on the approximate one-half of its surface viewed by the *NEAR* spacecraft (Veverka *et al.*, 1997). Substantial portions of the surfaces of Gaspra, Ida, and Mathilde are occupied by craters >2 km in diameter. Given that all three of these asteroids are probably substantially younger than Hebe, and given that the impacting flux was substantially higher during the early period of Hebe's existence, it is reasonable to expect that most of the surface of Hebe was impacted by projectiles with energy sufficient to produce impact-melt bodies in their craters.

Scaling the results of O'Keefe and Ahrens (1994) to typical asteroid impact velocities for their full range of model parameters

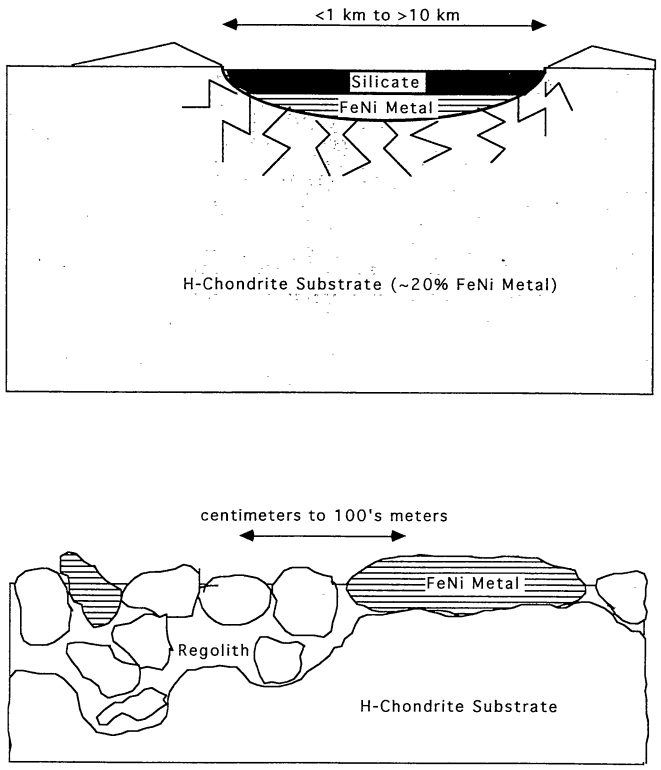

FIG. 10. (Top) Schematic model for the formation of metal-rich layers in the shallow subsurface of the H-chondrite and IIE iron meteorite parent body. The impact-melt sheet in the crater has differentiated into lower metal layer and upper silicate layer. Vertical scale and thickness of the melt layer is exaggerated. (Bottom) Schematic representation of the current Hebe surface layer. Impact gardening of surface has preferentially depleted weaker, brittle silicates while enriching stronger resistant metal at the surface.

(four orders of magnitude in their parameter, which incorporates melt enthalpy and yield strength) indicates melt sheets with thicknesses corresponding to 0.5–2.5% of the diameter of the associated crater. For a 10 km crater, this corresponds to melt sheet thicknesses of 50 to 250 m. For an average H-chondrite metal abundance of 18% (wt%), complete segregation of the metal would produce a metal layer 5 to 25 m thick at the base of such melt sheets. Incorporation of the FeS phase would increase their thicknesses by ~50%. (Note: Available spectral data suggest that FeS (troilite) is spectrally similar to Ni-Fe metal (Britt *et al.*, 1992) and, for purposes of our spectral discussion, is considered as metal.)

IS IMPACT MELTING A VIABLE MECHANISM ON ASTEROIDS?

Based upon cratering models, observations of terrestrial impact craters and lunar samples, and laboratory shock experiments, Keil *et al.* (1997) concluded that impacts cannot produce large-scale melting and whole-body differentiation. They also challenged the formation of impact-melt sheets in asteroidal craters and suggested that any impact melt volumes in asteroidal craters will be more than an order of magnitude smaller (*e.g.*, 0.01–0.1%) than that predicted by the equation of O'Keefe and Ahrens (1994). However, there are several lines of direct meteoritic evidence that suggest that impact melting is a significant localized process on asteroid surfaces. The presence of impact-melt rocks and clasts in the meteorite collections indicates that some effect must be operating to overcome the limitations outlined by Keil *et al.* (1997) in order to produce moderate amounts of impact melt during at least a subset of the large impacts onto asteroid surfaces.

Keil *et al.* (1997) noted that larger impact-melt volumes would be produced on targets that are anhydrous and on those that have porosity greater than the zero value used in their models. Water is absent on the H-chondrite parent body, and unweathered H chondrites have intrinsic porosities of ~10% (~90% of samples falling in the 5–20% range of porosity; Corrigan *et al.*, 1997; Consolmagno *et al.*, 1998). If—as now appears certain—there are substantial surface regoliths on the larger asteroids (Belton *et al.*, 1994), the bulk porosity (*i.e.*, intrinsic porosity plus regolith porosity) of the surface layer of Hebe must be substantial; it is almost certainly greater than the lower limit (23%) for the bulk porosity of asteroid Ida inferred from the Galileo flyby (23–73% depending on meteorite type and Ida mass; Belton *et al.*, 1995). The anhydrous and porous target rocks on the H-chondrite parent body should increase, perhaps substantially, the amount of impact melting over that estimated by Keil *et al.* (1997).

And finally, the IIE iron meteorites offer compelling evidence for a differentiation process related to impact heating. The range of IIE iron ages indicate that there were a series of melting and metal–silicate segregation events on the H-chondrite parent body (or its chemical, mineralogical, and isotopic twin) over a time interval from 4.5 Ga down to 3.7 Ga. There are only four plausible asteroid heating mechanisms (*e.g.*, Scott *et al.*, 1989; Rubin, 1995). Short-lived radioisotopes (such as ^{26}Al) and solar wind induction heating are the leading candidates for the cause of the magmatic activity that produced the igneous meteorites. However, these heating mechanisms are active only during the first few million years of solar system history. They cannot provide heating over the formation interval of the IIE iron meteorites. Heating due to decay of the long-lived radioisotopes (*e.g.*, ^{235}U, ^{238}U, ^{40}K, ^{234}Th) is significant only for the largest asteroids (*e.g.*, Scott *et al.*, 1989) and would not produce, or even approach, igneous temperatures in ~200 km diameter asteroids such as Hebe and the H-chondrite parent body. (Minster and Allegre (1979) suggested a possible diameter of 300 to 350 km for the H-chondrite parent body. From thermal models, Miyamoto *et al.* (1981) calculated a diameter of 170 km to match the metamorphic history of the H chondrites. From H-chondrite cooling rates and conductivities, Pellas and Fiéni (1988) inferred a diameter of 160 to 200 km for their parent body. On the basis of H-chondrite thermal histories, Bennett and McSween (1997) modeled the thermal evolution of the H-chondrite parent body and derived a diameter of 160 to 190 km. Akridge *et al.* (1998) concluded from thermal modeling that a Hebe-sized body was consistent with the thermal evolution of the H chondrites.) The temporal span of the heating events and the relatively small size of the potential parent bodies leave impacts as the only viable heat source for the igneous temperatures and metal–silicate differentiation recorded in the younger IIE iron meteorites.

Support for the impact-melt model is also found in the igneous inclusions in ordinary chondrite breccias (*e.g.*, Foder *et al.*, 1972; Foder and Keil, 1975; Wilkening, 1978; Rubin *et al.*, 1983; Sack *et al.*, 1994; Rubin, 1995; Yolcubal *et al.*, 1997; Ruzicka *et al.*, 1998 and references therein). Abundant examples of metal and sulfide-depleted silicate inclusions that have compositions similar to the silicates of their chondritic hosts are found in ordinary chondrites. What are seen in these igneous clasts are melts that formed very rapidly (to melt all phases simultaneously), underwent metal–silicate segregation, and quenched before the silicate could differentiate significantly. In their study of large (millimeter- to centimeter-scale)

igneous-textured clasts in the L3 meteorite Julesberg, Ruzicka *et al.* (1998) noted that these inclusions contain much less Ni-Fe metal (<0.06% up to 1.3%, median value = 0.26%) than the bulk meteorite (13.54%). These inclusions are similar in mineralogy and mineral composition to the upper silicate portions of the impact-melt sheets discussed above. Sack *et al.* (1994) concluded that two of the studied igneous inclusions from ordinary chondrites were samples of layered magma masses on the H-chondrite-like parent body that had segregated metal and sulfide from the silicates. Bridges and Hutchison (1997) concluded that a significant subset of clasts in ordinary chondrites were probably formed in impact-melt pools. The clasts studied by Ruzicka *et al.* (1998) required metal–silicate segregation on scales of at least centimeters and do not preclude segregation on much larger scales. At least some of the igneous-textured inclusions present in the ordinary chondrites were apparently excavated from solidified impact-melt masses that experienced metal–silicate segregation and distributed across the surface regolith of their parent body(s).

Despite the objections raised concerning the proposed impact heating mechanism to produce large metal masses on Hebe, there is compelling physical evidence (*i.e.*, there is no plausible asteroidal or meteorite parent-body heat source to produce IIE iron meteorites with ages of 4.4 to 3.7 Ga except impacts) that the proposed process actually operated on the H-chondrite parent body. Although the conditions that relaxed the constraints defined by Keil *et al.* (1997) are presently conjectural, there is strong evidence that they were relaxed in the case of the IIE iron parent body and the parent bodies of the ordinary chondrites that contain igneous clasts.

The meteorite evidence provides few constraints on the dimensions of the melt volumes. In many cases, they could be as small as a few centimeters ("pods" or "puddles") and still produce the observed igneous clasts. However, Keil *et al.* (1997) noted that the proportion of impact melt generated relative to the total crater volume increases significantly with increasing crater size. The abundance of igneous clasts in ordinary chondrite breccias and the abundance of the IIE iron meteorites (~0.12% of all falls, the eighth most abundant type of the eleven major iron meteorite types; Wasson, 1974) suggests that the production of impact melts is not uncommon. The range of formation ages among the IIE iron meteorites indicates samples from several distinct regions on their parent body, which again suggests that such regions are not extremely rare. Therefore we have chosen the "impact-melt sheet in crater bottoms" as our baseline model. That being the case, the previously derived thicknesses of metal layers associated with large craters on the surface of Hebe seems to be a reasonable initial estimate.

Alternatives to the Impact Melting Origin of the Surface Metal on Hebe

Localized melting on or within an otherwise unmelted chondritic parent body could also occur by other mechanisms. Herbert (1996, pers. comm.) has noted that if induction heating (*e.g.*, Herbert, 1989) operated on this asteroid, the spatial distribution of heating would probably be unstable against localized thermal runaway. This is due to the increase in electrical conductivity with temperature and the tendency of hot (more conductive) spots to divert current from neighboring cooler regions. This could produce a network of molten regions penetrating the unmelted (but probably metamorphosed) body of the asteroid. Differentiation should produce large lenticular pods of metal within the molten network. However, the young formation ages of some of the IIE iron meteorites would be difficult to reconcile with this mechanism.

In the previous discussion, it has been assumed that the IIE iron meteorites formed by impact melting and differentiation of an H-type assemblage. It has also been suggested that the IIE iron meteorites could have formed by accretion of a fragment of an iron core from a disrupted differentiated body (*e.g.*, Wasson and Wang, 1986; Casanova *et al.*, 1995). Most mesosiderites were apparently formed by just such a process, with the possible exception of type-4 mesosiderites that may have been derived from impact-melt sheets (*e.g.*, Rubin and Mittlefehldt, 1993). Solidification times of the magmatic iron meteorites are $<10^8$ years after solar system formation. Thus, if the younger IIE iron meteorites were formed by accretion of iron masses onto the IIE parent body, then impact heating must still be invoked to melt the solidified metal. The metallic core fragment might have still been relatively hot (even if solidified) which would have reduced the energy input needed to produce melting. However, if this is the origin of the H/IIE association, then there is the additional constraint provided by similarity of IIE metal to H-chondrite metal (*e.g.*, Wasson and Wetherill, 1979). That similarity would require that the impacting core fragment came from a differentiated parent body of H-chondrite composition, the probability of which cannot readily be estimated at the present time.

PRODUCING THE HEBE SURFACE ASSEMBLAGE

Thus we have three models to produce large metal masses on the H-chondrite parent body. Impact melting in large craters would result in Ni-Fe metal layers located below hundreds to thousands of meters of overburden, both the silicate part of the solidified melt sheet and fall back breccia. The "short-circuited" induction heating could produce pods of metal throughout the body. The accreted metal core fragment would produce surface and near-surface metal and metal–silicate masses. In the first two cases, the metal would have to be brought to the optical surface of the asteroid by removal of the overlying silicate layers. And in all three cases, regolith deposited from other impacts on the body's surface must be regularly removed from the metallic masses to keep them exposed at the optical surface.

Mean impact velocities onto the surface of Hebe (6.4 km/s; Rivkin and Bottke, 1996) are much higher than typical seismic (sound speed) velocities in ordinary chondrites (~2.1–4.2 km/s; Alexeyeva, 1960) and mafic silicate rocks (~3.5–5.5 km/s depending on porosity; Carmichael, 1982) but only slightly above the seismic velocities in Ni-Fe metal (5.8–6.3 km/s in iron and steel; Carmichael, 1982). From the velocity distributions of Rivkin and Bottke (1996), ~55% of the impacts onto the surface of Hebe will be above the mean seismic velocity of Ni-Fe metal (~6.0 km/s), ~67% will be above 5.5 km/s, and ~85% will be above 4.2 km/s. Impact velocities above the sound velocity of the target produce shock waves that tend to disaggregate and accelerate target material to relatively high velocities. The intensity of the shock and the mass of ejected target increases rapidly as the impact velocity exceeds the seismic velocity by a greater extent.

Moreover, the silicates are weaker than the metal phases, even when the metal phases are embrittled by low temperatures (*e.g.*, Gaffey, 1986 and references therein). So typical impacts (mostly supersonic) into the silicate portion (either the H-chondrite substrate or the upper silicate layers of melt bodies) of Hebe tend to fragment and eject these materials from the surface. Impacts onto the large metal masses (many subsonic) tend to locally deform them but are not nearly as efficient at fragmenting and ejecting the metal. Fragments of metal produced by these impacts will be larger than

the fragments of silicate. These larger metal fragments will tend to remain at the surface because they are more resistant to destruction by the smaller frequent impacts onto the surface. If there is seismic shaking of the regolith on these bodies due to impacts, the larger metal fragments will tend to migrate upward toward the surface, also increasing their optical effect.

The differential erosion can expose the buried metal layers and concentrates metal at the optical surface. The impacts comparable to the dimensions of the silicate layer overlying a metal layer are analogous to the lunar flat-bottomed and concentric craters formed by impactors striking a surface where a substantial regolith (with a thickness less than the crater depth) overlies a more competent bedrock or substrate (Oberbeck and Quaide, 1967; Quaide and Oberbeck, 1968). Due to the seismic velocity discontinuity at the interface, such impacts strip away large areas of the low-seismic velocity overburden but produce only small (or no) craters in the substrate. The effect is to strip away the overburden efficiently exposing the high-seismic velocity substrate. This provides a mechanism to remove both the initial overlying silicate layers in a melt sheet and to strip away regolith materials deposited on the exposed metallic surfaces by other impacts on the body.

Hydrocode models of impacts onto asteroid surfaces suggest that only the smallest bodies are in an erosive regime. However, the results of the *NEAR* encounter with asteroid 253 Mathilde (Veverka *et al.*, 1997; Asphaug, 1997) indicate situations where the hydrocode predictions do not adequately describe impacts onto asteroid surfaces and where much larger bodies are undergoing impact erosion.

The S-type spectrum of Hebe can be produced by a simple coarse-grained mixture of H-chondrite material (~60% by area) and Ni-Fe metal (~40% by area). In our preferred model outlined above, the metal derives from laterally extensive (hundreds to thousands of meters) but relatively thin (meters to tens of meters) metallic layers emplaced at shallow depths within large impact structures or possibly splashed across the surface by an impacting Ni-Fe core fragment. The metal has been exposed, concentrated, and maintained at the optical surface by differential impact erosion of the weaker and/or lower seismic velocity overlying silicate layers or regolith. Below this thin-metal-enriched surface layer, the bulk of the body of Hebe would be H-chondrite material.

Radar Tests of This Model

Chapman (1996) has pointed out that this interpretation should produce a diagnostic radar signature. Spatially resolved radar observations, obtainable with the upgraded Arecibo facility, could provide a good test of this interpretation. Until such data becomes available, the existing radar data can be examined.

Hebe has a radar albedo of 0.15, near the middle of the range for mainbelt S-type asteroids (Ostro *et al.*, 1991). The value for Hebe (and the other mainbelt S-asteroids) is lower than that of the mainbelt M-type asteroid (16 Psyche) with a probable metallic surface (0.26). As Ostro *et al.* (1985, 1991) has discussed, a plausible range of porosities on asteroid surfaces—the best estimate of a shallow regolith porosity (55%) is provided by the M asteroid 16 Psyche; Ostro *et al.* (1991)—allows considerable range in the metal abundance on S-asteroid surfaces. A porosity of 55% for the derived Hebe surface would be consistent with the measured radar albedo of this asteroid.

The circular polarization ratio of Hebe is 0.0—the lowest value for the S-asteroids (range = 0.0 to 0.32)—indicating that most of the radar return is single scattered from a surface that is smooth at the scale of the radar wavelength or from smooth surface elements with high radar albedos. Such a low circular polarization ratio has been considered to indicate a smooth surface at all scales within about an order of magnitude of the radar wavelength and an absence of centimeter-to-meter scale structures (*e.g.*, fragments) in the top few meters of regolith (Ostro *et al.*, 1991). The low circular polarization ratio of Hebe would also be consistent with the derived composition in which abundant metal slabs on the surface produce a large single-scattered radar component. Data from the upgraded Arecibo radar facility may provide a more definitive conclusion.

CONCLUSIONS

Several lines of evidence indicate that S(IV)-type asteroid 6 Hebe is the probable parent body of the H chondrites and the IIE iron meteorites. Hebe is located adjacent to both the ν_6 and 3:1 resonances and has been previously suggested as a major source of the terrestrial meteorite flux. The silicate portion of the surface assemblage of Hebe is consistent with the silicates in H chondrites. The high albedo of Hebe, relative to that of an H chondrite, rules out a lunar-style space weathering process as the mechanism producing the weakened absorption features and reddish spectral slope in the Hebe spectrum. Linear unmixing models show that the component, which produces the S-type spectrum of Hebe, is consistent with a typical Ni-Fe metal spectrum. Isotopic and petrographic evidence links the silicate-bearing IIE iron meteorites to the H-chondrite parent body. It is proposed that large impacts onto the relatively metal-rich H-chondrite target produced melt sheets, pools, or pods, which differentiated to form near-surface layers of metal. Alternately, masses of metal could have been added to the Hebe surface by the impact of a core or core fragment from a differentiated body of H-chondrite composition. Subsequent impacts preferentially eroded and depleted the overlying silicate components and regolith, concentrating and maintaining large masses of metal at the optical surface of Hebe.

The work described in the present paper has established the probable presence of an H-chondrite assemblage with abundant Ni-Fe masses on the surface of Hebe. Previous dynamical studies had established the viability of Hebe as a significant meteorite source. Previous linkages between the H chondrites and the IIE iron meteorites provided the basis for development of a mechanism to produce an S-type spectrum for a body with an H-chondrite composition. This mechanism may not work for the less metal-rich L chondrites and seems highly unlikely for the metal-poor LL chondrites. This mechanism cannot be generalized to other S(IV)-asteroids without careful spectral study of individual candidates.

Thus, Hebe is an object that apparently has the correct surface composition, for which a reasonable mechanism can be defined to produce the S-type spectrum, and from which we should be getting a substantial fraction of our meteorite flux. If the H-chondrite parent body is among the S-type asteroids, it will have to have all of these properties. If Hebe is not the H-chondrite parent body, then where are the meteorites from Hebe? Therefore we conclude that Hebe is the probable parent body of the H chondrites and the IIE iron meteorites. "Probable" means just that. Hebe is far and away the best candidate, but that does not mean that Hebe is the H-chondrite parent body beyond any doubt. The whole concept of probability (whether rigorously computed or expressed as relative likelihood) arose from studies of gambling. Probability never says "this is true" but only "that's the way to bet." We're betting on Hebe.

Acknowledgments–M. E. Gaffey is a visiting astronomer a the Infrared Telescope Facility that is operated by the University of Hawaii under contract to NASA. We wish to express our gratitude for the stimulating reviews of the original manuscript provided by Dan Britt and Clark Chapman. We are particularly grateful for additional comments provided by Paolo Farinella, Takahiro Hiroi, Fred Hörz, and Derek Sears. The paper benefited greatly from these inputs. Various aspects of this work were supported by NASA Planetary Geology and Geophysics grant NAGW-642 and by NSF Planetary Astronomy grant AST-9012180.

Editorial handling: R. P. Binzel

REFERENCES

AKRIDGE G., BENOIT P. H. AND SEARS D. W. G. (1998) Regolith and megaregolith formation of H-chondrites: Thermal constraints on the parent body. *Icarus* **132,** 185–195.

ALEXEYEVA K. N. (1960) New data on the physical properties of stony meeorites (in Russian). *Meteoritica* **18,** 68–76.

ASPHAUG E. (1997) New views of asteroids. *Science* **278,** 2070.

BELL J. F., DAVIS D. R., HARTMANN W. K. AND GAFFEY M. J. (1989) Asteroids: The big picture. In *Asteroids II* (eds. R. P. Binzel, T. Gehrels and M. S. Matthews), pp. 921–945. Univ. Arizona Press, Tucson, Arizona, USA.

BELTON M. J. S., CHAPMAN C. R., VEVERKA J., KLAASEN K. P., HARCH A., GREELEY R., GREENBERG R., HEAD J. W., III, MCEWEN A., MORRISON D., THOMAS P. C., DAVIS M. E., CARR M. H., NEUKUM G., FANALE F. P., DAVIS D. R., ANGER C., GIERASCH P. J., INGERSOLL A. P. AND PILCHER C. (1994) First images of asteroid 243 Ida. *Science* **265,** 1543–1547.

BELTON M. J. S., CHAPMAN C. R., THOMAS P. C., DAVIES M. E., GREENBERG R., KLAASEN K., BYRNES D., D'AMARIO L., SYNNOTT S., JOHNSON T. V., MCEWEN A., MERLINE W. J., DAVIS D. R., PETIT J-M., STORRS A., VEVERKA J. AND ZELLNER B. (1995) Bulk density of asteroid 243 Ida from the orbit of its satellite Dactyl. *Nature* **374,** 785–788.

BENNETT M. E., III AND MCSWEEN H. Y., JR. (1997) Revised model calculations for the thermal histories of ordinary chondrite parent bodies. *Meteorit. Planet. Sci.* **31,** 783–792.

BINZEL R. P. AND XU S. (1993) Chips off of asteroid 4 Vesta: Evidence for the parent body of basaltic achondrite meteorites. *Science* **260,** 186–191.

BINZEL R. P., XU S., BUS S. J., SKRUTSKIE M. F., MEYER M., KNEZEK P. AND BARKER E. S. (1993) The discovery of a main-belt asteroid resembling ordinary chondrite meteorites. *Science* **262,** 1541–1543.

BOGARD D. D., GARRISON D. H., NORMAN M., SCOTT E. R. D. AND KEIL K. (1995) ^{39}Ar-^{40}Ar age and petrology of Chico: Large-scale impact melting on the L chondrite parent body. *Geochim. Cosmochim. Acta* **59,** 1383–1399.

BRIDGES J. C. AND HUTCHISON R. (1997) A survey of clasts and large chondrules in ordinary chondrites. *Meteorit. Planet. Sci.* **32,** 389–394.

BRITT D. T. AND PIETERS C. M. (1991) Darkening in gas-rich ordinary chondrites: Spectral modelling and implications for the regoliths of ordinary chondrite parent bodies (abstract). *Lunar Planet. Sci.* **22,** 141–142.

BRITT D. T. AND PIETERS C. M. (1994) Darkening in black and gas-rich ordinary chondrites: The spectral effects of opaque morphology and distribution. *Geochim. Cosmochim. Acta* **58,** 3905–3919.

BRITT D. T., BELL J. F., HAACK H. AND SCOTT E. R. D. (1992) The reflectance spectrum of troilite (abstract). *Lunar Planet Sci.* **23,** 167–168.

BROGLIA P., MANARA A. AND FARINELLA P. (1994) Polarmetric observations of (6) Hebe. *Icarus* **109,** 204–209.

CARMICHAEL R. S., ED. (1982) *Handbook of Physical Properties of Rocks,* vol. II. CRC Press, Boca Raton, Florida, USA. 345 pp.

CASANOVA I., GRAF T. AND MARTI K. (1995) Discovery of an unmelted H-chondrite inclusion in an iron meteorite. *Science* **268,** 540–542.

CHAPMAN C. R. (1996) S-type asteroids, ordinary chondrites, and space weathering: The evidence from Galileo's fly-bys of Gaspra and Ida. *Meteorit. Planet. Sci.* **31,** 699–725.

CHAPMAN C. R. AND SALISBURY J. W. (1973) Comparisons of meteorite and asteroid spectral reflectivities. *Icarus* **19,** 507–522.

CHAPMAN C. R., MCCORD T. B. AND JOHNSON T. V. (1973) Asteroid spectral reflectivities. *Astron. J.* **78,** 126–140.

CHAPMAN C. R., VEVERKA J., THOMAS P. C., KLAASEN K., BELTON M. J. S., HARCH A., MCEWEN A., JOHNSON T. V., HELFENSTEIN P., DAVIS M. E., MERLINE W. J. AND DENK T. (1995) Discovery and physical properties of Dactyl, a satellite of asteroid 243 Ida. *Nature* **374,** 783–785.

CLARK B. E. (1995) Spectral mixing models of S-type asteroids. *J. Geophys. Res.* **100,** 14 443–14 456.

CLARK B. E. AND HIROI T. (1994) S-type asteroid spectral continua: Redness and Fe,Ni metal (abstract). *Bull. Am. Astron. Soc.* **26,** 1172.

CLARK B. E., FANALE F. P. AND SALISBURY J. W. (1992) Meteorite–asteroid spectral comparison: The effects of comminution, melting, and recrystallization. *Icarus* **97,** 288–297.

CLAYTON R. N., MAYEDA T. K., OLSEN E. AND PRINZ M. (1983) Oxygen isotope relationships in iron meteorites. *Earth Planet. Sci. Lett.* **65,** 229–232.

CLAYTON R. N., MAYEDA T. K., GOSWAMI J. N. AND OLSEN E. J. (1991) Oxygen isotope studies of ordinary chondrites. *Geochim. Cosmochim. Acta* **55,** 2317–2337.

CLOUTIS E., GAFFEY M. J., JACKOWSKI T. L. AND REED K. L. (1986) Calibration of phase abundance, composition, and particle size distribution for olivine–orthopyroxene mixtures from reflectance spectra. *J. Geophys. Res* **91,** 11 641–11 653.

CLOUTIS E. A., GAFFEY M. J., SMITH D. G. W. AND LAMBERT R. J. (1990) Metal–silicate mixtures: Spectral properties and applications to asteroid taxonomy. *J. Geophys. Res.* **95,** 8323–8338.

CONSOLMAGNO G. J. , BRITT D. T. AND STOLL C. P. (1998) The porosities of ordinary chondrites: Models and interpretations. *Meteorit. Planet. Sci.* **33,** 1221–1229.

CORRIGAN C. M., ZOLENSKY M. E., DAHL J., LONG M., WEIR J., SAPP C. AND BURKETT P. J. (1997) The porosity and permeability of chondritic meteorites and interplanetary dust particles. *Meteorit. Planet. Sci.* **32,** 509–515.

DODD R. T. (1981) *Meteorites, A Petrologic–Chemical Synthesis.* Cambridge Univ. Press, New York, New York, USA. 368 pp.

EBIHARA M., KONG P., IKEDA Y. AND KOJIMA H. (1996) Yamato 791093, an anomalous IIE iron (abstract). *Meteorit. Planet. Sci.* **31 (Suppl.),** A41.

FARINELLA P., GONCZI R., FROESCHLE CH. AND FROESCHLE C. (1993a) The injection of asteroid fragments into resonances. *Icarus* **101,** 174–187.

FARINELLA P., FROESCHLE C. AND GONCZI R. (1993b) Meteorites from the asteroid 6 Hebe. *Celest. Mech. Dynam. Astron.* **56,** 287–305.

FEIERBERG M. A., LARSON H. P. AND CHAPMAN C. R. (1982). Spectroscopic evidence for undifferentiated S-type asteroids. *Astrophys. J.* **257,** 361–372.

FISCHER E. M. AND PIETERS C. M. (1994) Remote determination of exposure degree and iron concentration of lunar soils using VIS-NIR spectroscopic methods. *Icarus* **111,** 475–488.

FODER R. V. AND KEIL K. (1975) Implications of poikilitic textures in LL-group chondrites. *Meteoritics* **10,** 325–339.

FODER R. V., KEIL K. AND JAROSEWICH E. (1972) The Oro Grande, New Mexico, chondrite and its lithic inclusion. *Meteoritics* **7,** 495–507.

GAFFEY M. J. (1976). Spectral reflectance characteristics of the meteorite classes. *J. Geophys. Res.* **81,** 905–920.

GAFFEY M. J. (1984) Rotational spectral variations of asteroid (8) Flora: Implications for the nature of the S-type asteroids and for the parent bodies of the ordinary chondrites. *Icarus* **60,** 83–114.

GAFFEY M. J. (1986) The spectral and physical properties of metal in meteoritic assemblages: Implications for asteroid surface materials. *Icarus* **66,** 468–486.

GAFFEY M. J. (1997) Surface lithologic heterogeneity of asteroid 4 Vesta. *Icarus* **127,** 130–157.

GAFFEY M. J. AND MCCORD T. B. (1979) Mineralogical and petrological characterizations of asteroid surface materials. In *Asteroids* (eds. T. Gehrels and M. S. Matthews), pp. 688–723. Univ. Arizona Press, Tucson, Arizona, USA.

GAFFEY M. J., BELL J. F. AND CRUIKSHANK D. P. (1989) Reflectance spectroscopy and asteroid surface mineralogy. in *Asteroids II* (eds. R. P. Binzel, T. Gehrels and M. S. Matthews), pp. 98–127. Univ. Arizona Press, Tucson, Arizona, USA.

GAFFEY M. J., REED K. L. AND KELLEY M. S. (1992) Relationship of E-type Apollo asteroid 3103 (1982 BB) to the enstatite achondrite meteorites and the Hungaria asteroids. *Icarus* **100,** 95–109.

GAFFEY M. J., BURBINE T. H. AND BINZEL R. P. (1993a) Asteroid spectroscopy and the meteorite connection: Progress and perspectives. *Meteoritics* **28,** 161–187.

GAFFEY M. J., BELL J. F., BROWN R. H., BURBINE T. H., PIATEK J., REED K. L. AND CHAKY D. A. (1993b) Mineralogic variations within the S-type asteroid class. *Icarus* **106,** 573–602.

GEHRELS T. AND TAYLOR R. C. (1977) Minor planets and related objects. XXII. Phase functions for (6) Hebe. *Astron. J.* **82,** 229–237.

HERBERT F. (1989) Primordial electrical induction heating of asteroids. *Icarus* **78,** 402–410.

HIROI T., BELL J. F., TAKEDA H. AND PIETERS C. M. (1993) Modeling of S-type asteroid spectra using primitive achondrites and iron meteorites. *Icarus* **102,** 107–116.

KEIL K., BELL J. F. AND BRITT D. T. (1992) Reflection spectra of shocked ordinary chondrites and their relationship to asteroids. *Icarus* **98,** 43–53.

KEIL K., STÖFFLER D., LOVE S. G. AND SCOTT E. D. R. (1997) Constraints on the role of impact heating and melting in asteroids. *Meteorit. Planet. Sci.* **32,** 349–363.

LAGERKVIST C-I., BARUCCI M. A., CAPRIA M. T., FULCHIGNONI M., GUERRIERO L., PEROZZI E. AND ZAPPALÀ V. (1987) *Asteroid Photometric Catalogue*. Consiglio Nazionale Delle Ricerche, Inst. di Astrofisica Spaziale, Rome, Italy. 580 pp.

LAGERKVIST C-I., HARRIS A. W. AND ZAPPALA V. (1989) Asteroid lightcurve parameters. In *Asteroids II* (eds. R. P. Binzel, T. Gehrels and M. S. Matthews), pp. 1162–1179. Univ. Arizona Press, Tucson, Arizona, USA.

MAGNUSSON P. (1986) Distribution of spin axes and senses of rotation for 20 large asteroids. *Icarus* **68,** 1–39.

MCCORD T. B. (1968). A double beam astronomical photometer. *Appl. Opt.* **7,** 475–478.

MCCORD T. B. AND GAFFEY M. J. (1974). Asteroids: Surface composition from reflection spectroscopy. *Science* **186,** 352–355.

MCCOY T. J., KEIL K., CLAYTON R. N., MAYEDA T. K., BOGARD D. D., GARRISON D. H. AND WIELER R. (1997a) A petrologic and isotopic study of lodranites: Evidence for early formation as partial melt residues from heterogeneous precursors. *Geochim. Cosmochim. Acta* **61,** 623–637.

MCCOY T. J., KEIL K., MUENOW D. W. AND WILSON L. (1997b) Partial melting and melt migration in the acapulcoite-lodranite parent body. *Geochim. Cosmochim. Acta* **61,** 639–650.

MCSWEEN H. Y., JR. AND LABOTKA T. C. (1993) Oxidation during metamorphism of the ordinary chondrites. *Geochim. Cosmochim. Acta* **57,** 1105–1114.

MCSWEEN H. Y., JR., BENNETT M. E., III AND JAROSEWICH E. (1991) The mineralogy of ordinary chondrites and implications for asteroid spectrophotometry. *Icarus* **90,** 107–116.

MICHALOWSKI T. (1988) Photometric astrometry applied to asteroids: 6, 15, 43, and 624. *Acta Astron.* **38,** 455–468.

MIGLIORINI F., MANARA A., SCALTRITI F., FARINELLA P., CELLINO A. AND DI MARTINO M. (1997) Surface properties of (6) Hebe: A possible parent body of ordinary chondrites. *Icarus* **128,** 104–113.

MINSTER J-F. AND ALLÈGRE C. J. (1979) ^{87}Rb-^{87}Sr chronology of H chondrites: Constraint and speculations on the early evolution of their parent body. *Earth Planet. Sci. Lett.* **42,** 333–347.

MITTLEFEHLDT D. W., LINDSTROM M. M., BOGARD D. D., GARRISON D. H. AND FIELD S. W. (1996) Acapulco- and Lodran-like achondrites: Petrology, geochemistry, chronology, and origin. *Geochim. Cosmoschim. Acta* **60,** 867–882.

MIYAMOTO M., FUJII N. AND TAKEDA H. (1981) Ordinary chondrite parent body: An internal heating model. *Proc. Lunar Planet. Sci. Conf.* **12th,** 1145–1152.

MORBIDELLI A., GONCZI R., FROESCHLE CH. AND FARINELLA P. (1994) Delivery of meteorites through the ν_6 secular resonance. *Astron. Astrophys.* **282,** 955–979.

MOROZ L. V., FISENKO A. V., SEMJONOVA L. F., PIETERS C. M. AND KOROTAEVA N. N. (1996) Optical effects of regolith processes on S-asteroids as simulated by laser shots on ordinary chondrite and other mafic materials. *Icarus* **122,** 366–382.

OBERBECK V. R. AND QUAIDE W. L. (1967) Estimated thickness of a fragmental surface layer of Oceanus Procellarium. *J. Geophys. Res.* **72,** 4697–4704.

O'KEEFE J. D. AND AHRENS T. J. (1994) Impact-induced melting of planetary surfaces. In *Large Meteorite Impacts and Planetary Evolution* (eds. B. O. Dressler, R. A. F. Grieve and V. L. Sharpton), pp. 103–109. Geol. Soc. Am. Special Paper **293,** Boulder, Colorado, USA.

OLSEN E., DAVIS A., CLARKE R. S., JR., SCHULTZ L., WEBER H. W., CLAYTON R., MAYEDA T., JAROSEWICH E., SYLVESTER P., GROSSMAN L., WANG M-S., LIPSCHUTZ M. E., STEELE I. M. AND SCHWADE J. (1994) Watson: A new link in the IIE iron chain. *Meteoritics* **29,** 200–213.

OSTRO S. J., CAMPBELL D. B. AND SHAPIRO I. I. (1985) Mainbelt asteroids: Dual-polarization radar observations. *Science* **229,** 442–446.

OSTRO S. J., CAMPBELL D. B., CHANDLER J. F., HINE A. A., HUDSON R. S., ROSEMA K. D. AND SHAPIRO I. I. (1991) Asteroid 1986 DA: Radar evidence for a metallic composition. *Science* **252,** 1399–1404.

PELLAS P. AND FIÉNI C. (1988) Thermal histories of ordinary chondrite parent asteroids (abstract). *Lunar Planet. Sci.* **19,** 915–916.

QUAIDE W. L. AND OBERBECK V. R. (1968) Thickness determinations of the Lunar surface layer from Lunar impact craters. *J. Geophys. Res.* **73,** 5247–5270.

RIVKIN A. S. AND BOTTKE W. F. (1996) Hypervelocity impacts in the asteroid belt (abstract). *Lunar Planet. Sci.* **27,** 1077–1078.

RUBIN A. E. (1995) Petrologic evidence for collisional heating of chondritic asteroids. *Icarus* **113,** 156–167.

RUBIN A. E. AND MITTLEFEHLDT D. W. (1993) Evolutionary history of the mesosiderite asteroid: A chronologic and petrologic synthesis. *Icarus* **101,** 201–212.

RUBIN A. E., REHFELDT A., PETERSON E., KEIL K. AND JAROSEWICH E. (1983) Fragmental breccias and the collisional evolution of ordinary chondrite parent bodies. *Meteoritics* **18,** 179–196.

RUBIN A. E., JERDE E. A., ZONG P., WASSON J. T., WESTCOTT J. W., MAYEDA T. K. AND CLAYTON R. N. (1986) Properties of the Guin ungrouped iron meteorite: The origin of Guin and of group-IIE irons. *Earth Planet. Sci. Lett.* **76,** 209–226.

RUZICKA A., SNYDER G. A. AND TAYLOR L. A. (1998) Mega-chondrules and large, igneous-textured clasts in Julesberg (L3) and other ordinary chondrites: Vapor-fractionation, shock-melting, and chondrule formation. *Geochim. Cosmochim. Acta* **62,** 1419–1442.

SACK R. O., GHIORSO M. S., WANG M-S. AND LIPSCHUTZ M. E. (1994) Igneous inclusions from ordinary chondrites: High temperature cumulates and a shock melt. *J. Geophys. Res.* **99,** 26 029–26 044.

SCOTT E. D. R., TAYLOR G. J., NEWSOM H. E., HERBERT F., ZOLENSKY M. AND KERRIDGE J. F. (1989) Chemical, thermal and impact processing of asteroids. In *Asteroids II* (eds. R. P. Binzel, T. Gehrels and M. S. Matthews), pp. 701–739. Univ. Arizona Press, Tucson, Arizona, USA.

TAKEDA H., MORI H., HIROI T. AND SAITO J. (1994) Mineralogy of new Antarctic achondrites with affinity to Lodran and a model of their evolution in an asteroid. *Meteoritics* **29,** 830–842.

TAYLOR G. J. (1992) Core formation in asteroids. *J. Geophys. Res.* **97,** 14 717–14 726.

TEDESCO E. F., WILLIAMS J. G., MATSON D. L., VEEDER G. J., GRADIE J. C. AND LEBOFSKY L. A. (1989) A three-parameter asteroid taxonomy. *Astron. J.* **97,** 580–606.

TEDESCO E. F., VEEDER G. J., FOWLER J. W. AND CHILLEMI J. R. (1992) *The IRAS Minor Planet Survey*. JPL, PL-TR-92-2049, Phillips Lab., Air Force Material Command, Hanscom Air Force Base, Massachusetts, USA. 437 pp.

VEVERKA J., THOMAS P., HARCH A., CLARK B., BELL J. F., III, CARCICH B., JOSEPH J., CHAPMAN C., MERLINE W., ROBINSON M., MALIN M., MCFADDEN L. A., MURCHIE S., HAWKINS S. E., III, FARQUHAR R., IZENBERG N. AND CHENG A. (1997) NEAR's flyby of 253 Mathilde: Images of a C asteroid. *Science* **278,** 2109–2114.

WASSON J.T. (1974) *Meteorites*. Springer-Verlag, New York, New York, USA. 316 pp.

WASSON J. T. AND WANG J. (1986) A nonmagmatic origin of group-IIE iron meteorites. *Geochim. Cosmochim. Acta* **50,** 725–732.

WASSON J. T. AND WETHERILL G. W. (1979) Dynamical, chemical and isotopic evidence regarding the formation locations of asteroids and meteorites. In *Asteroids* (eds. T. Gehrels and M. S. Matthews), pp. 926–974. Univ. Arizona Press, Tucson, Arizona, USA.

WETHERILL G. W. AND CHAPMAN C. R. (1988) Asteroids and meteorites. In *Meteorites and the Early Solar System* (eds. J. F. Kerridge and M. S. Matthews), pp. 35–67. Univ. Arizona Press, Tucson, Arizona, USA.

WILKENING L. L. (1978) Tysnes Island: An unusual clast composed of solidified, immiscible, Fe-FeS and silicate melt. *Meteoritics* **13,** 1–9.

WILLIAMS J. G. (1973) Meteorites from the asteroid belt (abstract). *EOS (Trans. Am. Geophys. Union)* **54,** 233.

WILLIAMS J. G. AND FAULKNER J. (1981) The position of secular resonance surfaces. *Icarus* **46,** 390–399.

WISDOM J. (1985) A perturbative treatment of motion near the 3/1 commensurability. *Icarus* **63,** 272–289.

XU S., BINZEL R. P., BURBINE T. H. AND BUS S. J. (1995) Small main-belt asteroid spectroscopic survey: Initial results. *Icarus* **115,** 1–35.

YOLCUBAL I., SACK R. O., WANG M-S. AND LIPSCHUTZ M. E.(1997) Formation conditions of igneous regions in ordinary chondrites: Chico, Rose City, and other heavily shocked H and L chondrites. *J. Geophys. Res.* **102,** 21 589–21 611.

ZAPPALÀ V. AND KNEZEVIC Z. (1984) Rotation axes of asteroids: Results for 14 objects. *Icarus* **59,** 436–455.